Originally published as:

Insights into spatial sensitivities of ice mass response to environmental change from the SeaRISE ice sheet modeling project II: Greenland

Sophie Nowicki,[1] Robert A. Bindschadler,[1] Ayako Abe-Ouchi,[2] Andy Aschwanden,[3] Ed Bueler,[3] Hyeungu Choi,[4] Jim Fastook,[5] Glen Granzow,[6] Ralf Greve,[7] Gail Gutowski,[8] Ute Herzfeld,[9] Charles Jackson,[8] Jesse Johnson,[6] Constantine Khroulev,[3] Eric Larour,[10] Anders Levermann,[11] William H. Lipscomb,[12] Maria A. Martin,[11] Mathieu Morlighem,[13] Byron R. Parizek,[14] David Pollard,[15] Stephen F. Price,[12] Diandong Ren,[16] Eric Rignot,[10,13] Fuyuki Saito,[17] Tatsuru Sato,[7] Hakime Seddik,[7] Helene Seroussi,[10] Kunio Takahashi,[17] Ryan Walker,[1,18] and Wei Li Wang[1]

[1]   The Sea-level Response to Ice Sheet Evolution (SeaRISE) effort explores the sensitivity of the current generation of ice sheet models to external forcing to gain insight into the potential future contribution to sea level from the Greenland and Antarctic ice sheets. All participating models simulated the ice sheet response to three types of external forcings: a change in oceanic condition, a warmer atmospheric environment, and enhanced basal lubrication. Here an analysis of the spatial response of the Greenland ice sheet is presented, and the impact of model physics and spin-up on the projections is explored. Although the modeled responses are not always homogeneous, consistent spatial trends emerge from the ensemble analysis, indicating distinct vulnerabilities of the Greenland ice sheet. There are clear response patterns associated with each forcing, and a similar mass loss at the full ice sheet scale will result in different mass losses at the regional scale, as well as distinct thickness changes over the ice sheet. All forcings lead to an increased mass loss for the coming centuries, with increased basal lubrication and warmer ocean conditions affecting mainly outlet glaciers, while the impacts of atmospheric forcings affect the whole ice sheet.

1. Introduction

[2]   To correctly forecast sea level evolution, ice sheet models need to accurately predict the response of the Greenland and Antarctic ice sheets to their surrounding environments. For the Greenland ice sheet, these responses include, for example, the recently observed ice velocity speedup [*Rignot and Kanagaratnam*, 2006; *Joughin et al.*,

---

2004], the retreat and thinning of marine terminating glaciers [e.g., *Howat et al.*, 2007; *Howat and Eddy*, 2011; *Luckman et al.*, 2006; *van den Broeke et al.*, 2009; *Joughin et al.*, 2012], and the thickness change and mass loss measured by satellite altimetry, interferometry, and gravimetry [*Pritchard et al.*, 2009; *Zwally et al.*, 2011; *Velicogna*, 2009; *Rignot et al.*, 2011; *Shepherd et al.*, 2012]. Numerical simulation of these observed phenomena requires not only ice sheet models to capture the rapid dynamic changes of outlet glaciers, which requires ice sheet models to simulate marine terminating ice front evolution at the relevant spatial and temporal scales, but also an accurate prescription of the climatic forcing that drives the observed responses. Feedbacks between ice sheets and climate will in turn likely influence the future evolution of these systems, such that accurate quantitative predictions of future sea levels will ultimately require simulation of ice sheet evolution in fully coupled atmospheric and oceanic climate models.

[3] Efforts of including dynamic ice sheet models in global climate models are underway [e.g., *Little et al.*, 2007; *Lipscomb et al.*, 2009]. However, this two-way coupling is still in its infancy, such that ice sheet models are, at the moment, mostly driven offline by the outputs from global climate models [e.g., *Stone et al.*, 2010]. However, the cause of the observed dynamic changes and their link to the climate are often under debate. For example, the correlation between observed ice speed up and surface melt water suggested that moulin drainage lead to increased lubrication of basal ice [*Zwally et al.*, 2002; *Joughin et al.*, 2008a; *Shepherd et al.*, 2009; *Bartholomew et al.*, 2010], but recent theoretical advances [*Schoof*, 2010] demonstrate that increased surface melt can lead to slowdown rather than speedup and that ice speedup is mostly driven by water variability. Ice speedup has also been attributed to ice-ocean interaction in marine terminating glaciers [*Joughin et al.*, 2008b; *Holland et al.*, 2008; *Vieli and Nick*, 2011; *Moon et al.*, 2012]. It is thus still unclear how to spatiotemporally parameterize the relevant processes in whole ice sheet models, with the result that the present generation of ice sheet models does not incorporate crucial subgrid processes. Furthermore, the current conditions beneath the ice sheet are poorly constrained due to the remoteness of the subglacial environment. Basal topography and ice thickness, for example, determine ice sheet volume [*Stone et al.*, 2010], are a first-order control on ice dynamics [*Larour et al.*, 2012a], influence the thermal and velocity regimes of the ice sheets [*van der Veen and Payne*, 2004], and are thus of crucial significance. Basal sliding is also poorly understood as it cannot be directly measured and has to be inferred using data assimilation techniques [*MacAyeal*, 1989]. Thus, accurate predictions of future sea level require not only further theoretical and numerical developments but also field and remote sensing observations.

[4] Despite these limitations, the current ice sheet models still provide valuable information on the potential response and sensitivity of the Greenland ice sheet to future climatic conditions. As described by *Bindschadler et al.* [2013], the Sea-level Response to Ice Sheet Evolution effort (SeaRISE) was designed to examine the sensitivity of the current spectrum of ice sheet models to prescribed external forcings. The sensitivity experiments were designed by the community of modelers that participated in SeaRISE and had to be simple enough for all models to implement. Three distinct types of forcing were considered: (i) the potential effect of enhanced marine melt, (ii) the effect of a warmer atmosphere on surface mass balance, and (iii) their indirect effect via enhanced basal sliding conditions. In its later stage, SeaRISE designed a final experiment (the R8 experiment in *Bindschadler et al.* [2013]) that attempts to quantify a more plausible future scenario for the coming 500 years, with present day set at 1 January 2004.

[5] To mitigate model differences due to inputs that could be standardized, existing data such as surface elevation [*Bamber et al.*, 2001a, 2001b], surface velocities [*Joughin et al.*, 2010], and basal heat flux [*Shapiro and Ritzwoller*, 2004] were combined into a single data set on a common 5×5 km grid, made available to any modeling group (see *Bindschadler et al.* [2013] or http://websrv.cs.umt.edu/isis/index.php/Data). In addition, the recent NASA Operation IceBridge and Center for Remote Sensing of Ice Sheets (CReSIS) bedrock data over four outlet glaciers [*Herzfeld et al.*, 2012] were incorporated into the bedrock topography of *Bamber et al.* [2001a, 2001b]. The SeaRISE modelers agreed upon a standard output consisting of selected variables at 5 year intervals. The output grid is consistent with the input data set and required models with a coarser/denser resolution to interpolate/aggregate their results onto the 5×5 km grid.

[6] The eight models taking part in the Greenland suite of SeaRISE experiments are the Anisotropic Ice Flow model (AIF) [*Wang et al.*, 2012], the Community Ice Sheet Model version 2 (CISM2) [*Price et al.*, 2011; *Lemieux et al.*, 2011; *Evans et al.*, 2012; *Bougamont et al.*, 2012], the Elmer/Ice model [*Seddik et al.*, 2012], the Ice sheet model for Integrated Earth-System Studies (IcIES) [*Saito and Abe-Ouchi*, 2004, 2005, 2010; *Greve et al.*, 2011], the Ice Sheet System Model (ISSM) [*Morlighem et al.*, 2010; *Seroussi et al.*, 2011; *Larour et al.*, 2012b], the Parallel Ice Sheet Model (PISM) [*Bueler and Brown*, 2009; *Aschwanden et al.*, 2012], the Simulation Code for POLythermal Ice Sheet (SICOPOLIS) [*Greve*, 1997; *Greve et al.*, 2011], and the University of Maine Ice Sheet Model (UMISM) [*Fastook*, 1993; *Fastook and Hughes*, 1990; *Fastook and Prentice*, 1994]. The essential features of these eight models are summarized in Table A1 in Appendix A and in more detail in *Bindschadler et al.* [2013]. The models taking part in SeaRISE thus represent the current spectrum of ice sheet models and range from shallow ice models to the more complex full-Stokes model Elmer/Ice. SeaRISE's models therefore differ not only in their physical sophistication and components, but also in terms of spatial and temporal resolution. However, it is not clear that higher complexity makes a model a better predictor of future evolution, since other factors such as initialization also come into play. Therefore, it is argued that one strength of SeaRISE is the inclusion of a variety of ice sheet models and initialization processes. This approach reflects the Intergovernmental Panel on Climate Change (IPCC) multiple model examination of the possible range of global climate response to various emission scenarios [*Intergovernmental Panel on Climate Change (IPCC)*, 2007] and that "no minimum performance" requirement should be imposed on climate models for inclusion in the Coupled Model Intercomparison Phase 5 effort [*Knutti et al.*, 2010a], which will form the basis of climate projections for the IPCC Fifth Assessment Report (AR5).
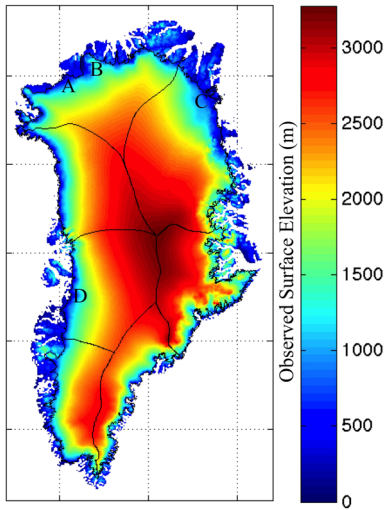
Figure 1. Observed surface elevation of modern-day Greenland [*Bamber et al.*, 2001a, 2001b] Drainage divides (black lines) are shown for the seven basins, along with location of the glaciers (dot) discussed in the text. Basins clockwise from the north: 1. north basin, 2. north east basin, 3. central east basin, 4. south east basin, 5. south west basin, 6. central west basin, and 7. north west basin. Glaciers: A. Humboldt, B. Petermann, C. Nioghalvferdsbrae, D. Jakobshavn Isbrea.

[7] *Bindschadler et al.* [2013] concentrate on the temporal evolution of the ice volume resulting from the SeaRISE experiment and show that for a given forcing (atmospheric, oceanic, or basal sliding) the simulated responses exhibit behaviors that are similar across the models, though varying in magnitude. All forcings result in a mass loss from the Greenland ice sheet, but the mass loss occurs at different rates and time scales. The climate forcing leads to an initial small decay that later rapidly accelerates. In contrast, the dynamical experiments in the form of ocean melt rate and enhanced basal sliding initially respond faster than the climatic forcing and later decelerate. In addition, summing the ice volume temporal responses from individual forcings provides a close approximation to the response of combination experiments, where multiple forcings are imposed simultaneously.

[8] The primary purpose of this paper is to investigate the spatial response of the Greenland ice sheet to the simple SeaRISE forcings at specific times in order to gain insight into the changes in ice volume reported in *Bindschadler et al.* [2013]. Our goal is to explore the impact of model physics, implementation of forcings and spin-up on projections, and thus to document improvements in experimental procedure or in ice sheet models that would benefit future modeling efforts such as SeaRISE. Here we focus on the spatial characteristics of the ice thickness response as an ensemble unweighted multimodel mean, rather than on individual model responses. When combined with other statistical information such as standard deviation, the ensemble means not only capture the general trends but also identify where models agree or disagree [*Gates et al.*, 1999] and can guide where efforts are best spent to improve models [*Knutti et al.*, 2010b]. Although considering a subset of models, or weighting multi-model means, can improve

the reliability of weather and climate predictions [e.g., *Stephenson et al.*, 2005], evaluating the skill of models is difficult, as different metrics produce different rankings of climate models considered [*Gleckler et al.*, 2008]. The lack of a robust approach in assigning weights to climate models is problematic [*Knutti et al.*, 2010a], as inappropriate weighting can lead to more information being lost rather than could potentially be gained by suitable weighting [*Weigel et al.*, 2010]. In addition, focusing on specific model skills may lead to overconfidence and convergence that is unjustified [*Knutti et al.*, 2010a]. When combining multimodel climate projections, *Knutti et al.* [2010a] therefore recommend in the first instance that all models are used in the ensemble without ranking or assigning weights. The strength of an unweighted ensemble analysis is that it allows an estimate of the sensitivity to the prescribed forcings to be evaluated as broadly as possible, through the inclusivity of a diversity of models. On the other hand, the weakness of such an approach lies in the difficulty of evaluating the absolute accuracy of each of the models involved and therefore their aggregate ensemble projection. Therefore, in acknowledgment that the unweighted ensemble approach hides the actual response of each model and that there is no guarantee that the ensemble trend is more likely than any single realization [e.g., *Giorgi*, 2005], the behaviors of the models that are the least and the most sensitive to the experiment will also be explored, and the responses of all models are shown in the supporting information.

[9] The ice sheet models that constitute the Greenland component of SeaRISE are presented in section 2, where the problem of obtaining an initial configuration is discussed. The SeaRISE sensitivity experiments considered in this study are introduced in section 3. The sensitivity of the ice sheet to the simple forcings is introduced in section 4 with a basin analysis of the change in ice volume and further explored in sections 5 where we focus on the patterns of thickness change associated with each forcing. The paper concludes in section 10 with a summary and a discussion of the implication of our findings for future forecasting efforts of sea level from ice sheet models.

2. SeaRISE Experiments Initial Configuration

[10] Prognostic simulations of future ice response first require a determination of the present day state of the ice sheet. Two distinct methods are currently used by ice sheet models: long interglacial "spin-ups," and initialization using data assimilation of present-day observations. Both methods have advantages and drawbacks. The interglacial spin-ups allow fields to be dependent on the long-term memory of the ice sheet, such as internal temperature [*Rogozhina et al.*, 2011], and contain a representation of internal transients. However, the resulting configuration might differ from the currently observed state of the ice sheet. In contrast, ice sheet models that are initialized with observed surface elevation and thicknesses closely match the current state of the ice sheet, but lack dependence on its history. Inconsistencies in present-day data sets also limit the reliability of projections from such models, as models that are initialized with data assimilation to reproduce the present-day conditions start by artificially redistributing the glacier mass to reconcile
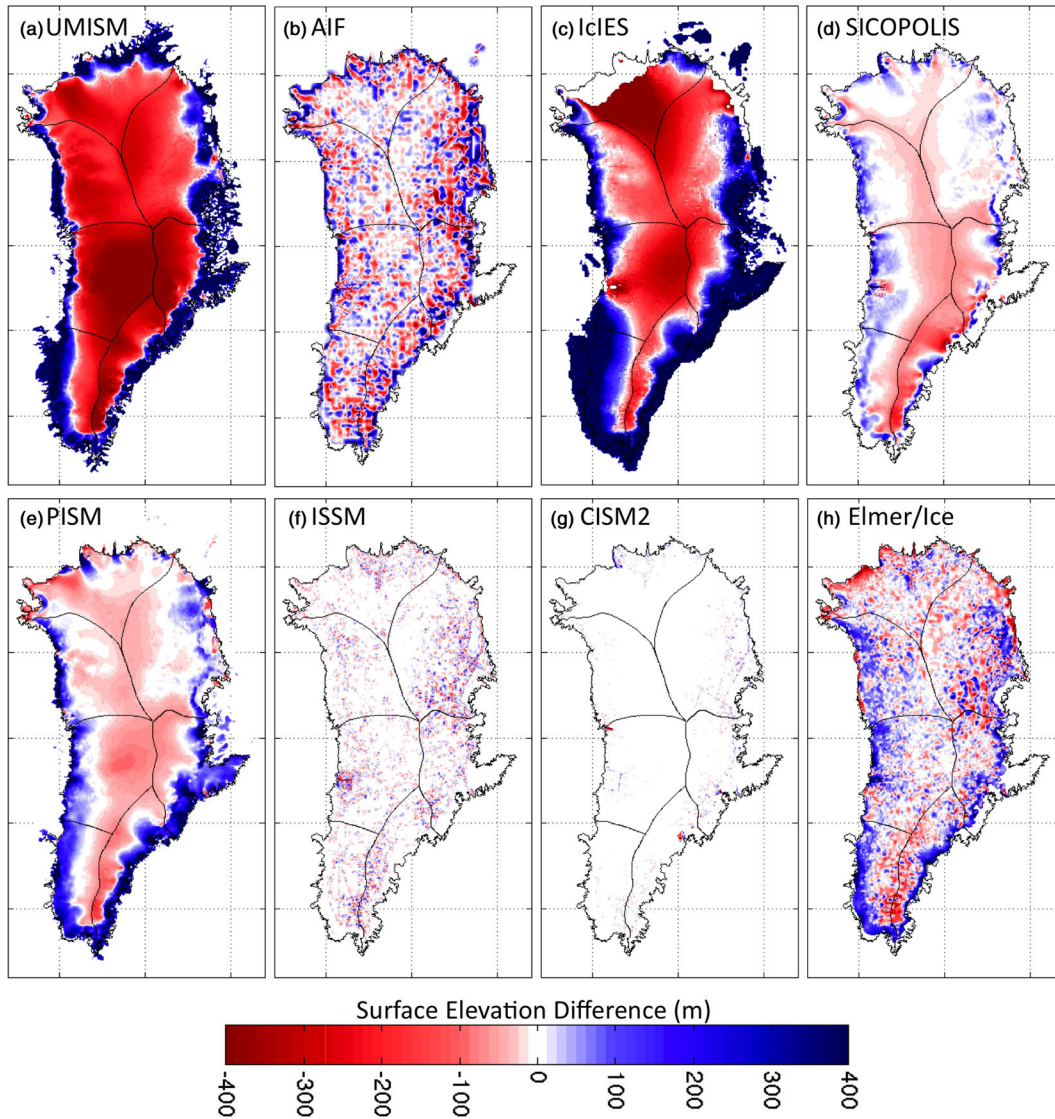
Figure 2. Difference in surface elevation between the SeaRISE ice sheet model initial conditions and modern-day Greenland.

these inconsistencies [*Seroussi et al.*, 2011]. Assimilation methods that do not account for the current climatic trends and surface mass balance can thus force ice sheet models far from equilibrium with the climate, and unnatural transients can emerge as the initial state evolves during prognostic modeling occurs.

[11] The observed ice sheet surface [*Bamber et al.*, 2001a, 2001b] provided as a reference in the SeaRISE data set (5 km × 5 km grid) and shown in Figure 1 is compared to the starting configuration for the SeaRISE experiments in Figure 2, in order to illustrate the result of the various initialization processes. The three models that initialize with present-day observations, AIF, CISM2, and ISSM, show little deviation from the reference surface elevation data, since the assimilation procedure holds the ice sheet geometry fixed to that of the present day. ISSM uses formal inverse methods [*MacAyeal*, 1989; *Morlighem et al.*, 2010] to infer the basal friction such that the resulting velocities match the present-day interferometric synthetic aperture radar velocities, and

computes the initial temperature assuming steady state. CISM2 tunes the basal friction coefficients so that modeled depth-averaged velocities are a good match to the balance velocities [*Price et al.*, 2011], with the latter calculated from the initial ice sheet geometry and surface mass balance fields. The basal friction coefficients are iteratively adjusted while the internal temperatures and velocities are evolved to a quasi-steady state. AIF uses balance velocities to tune the enhancement factor (a parameter allowing anisotropic flow) and initializes using the present day climate [*Wang et al.*, 2012]. In Figure 2, the difference between the reference surface elevations data and the initial configurations of models that initialize with assimilation methods is due to interpolations between the reference grid and the model meshes; in particular, the blocky nature of AIF along the ice sheet perimeter is a result of the coarse grid size (40 km) used by this model.

[12] In contrast, the four models that carried out interglacial spin-ups, namely, IcIES, PISM, SICOPOLIS, and UMISM,

Table 1. Initial Volume Above Flotation in Centimeter Sea-Level Equivalent (SLE), and Associated Change (Experiment-Control) After 100 Years of SeaRISE Sensitivity Experiments[a]

Experiment	UMISM	AIF	IcIES	SICOPOLIS	PISM	ISSM	CISM2	Elmer/Ice	Mean
Initial	695	712	755	707	725	710	709	718	717
CC-Initial	−0.25	3.0	−0.07	−2.46	−0.90	4.99	−0.77	6.18	1.22
C1-CC	−3.67	−2.82	−6.48	−2.16	−5.98	−1.68	−0.90	−2.13	−3.23
C2-CC	−5.63	−6.20	−12.21	−4.37	−12.12	−2.44	−1.33	−4.20	−6.06
C3-CC	−7.42	−11.67	−20.20	−7.79	−21.14	−3.16	−1.68	−7.39	−10.06
S1-CC	−10.74	−3.46	−3.70	−9.12	−1.54	−6.13	−6.76	−12.84	−6.79
S2-CC	−15.15	−5.16	−5.16	−13.00	−2.18	−9.18	−9.87	−22.65	−10.29
S3-CC	−22.19	−6.79	−6.38	−16.80	−2.82	−12.11	−12.78	−34.62	−14.31
M1-CC	−12.35	−0.21	−0.22	−0.68	X	−0.01	X	X	−2.24
M2-CC	−57.48	−4.29	−2.90	−1.01	X	−1.02	X	X	−11.11
M3-CC	−82.34	−10.81	−15.97	−12.36	X	−1.60	X	X	−20.51
S1C1-CC	−13.82	−6.49	−10.71	−11.17	−7.63	−7.67	−7.77	−15.01	−10.03

[a]X indicates no submission from the model.

deviate from the reference data, an effect seen in both the spatial extent and elevation. The different techniques for interglacial spin-ups play an important role. UMISM's spin-up used ice core proxy temperature [*Johnsen et al.*, 1995] to drive a 30 kyr variable climate [*Box and Steffen*, 2001, *van der Veen et al.*, 2001; *Fausto et al.*, 2009; *Burgess et al.*, 2010], with no tuning used to force the ice sheet toward the present-day configuration. The outcome is a thicker peripheral ice mass combined with a thinner interior. IcIES and SICOPOLIS paleoclimatic spin-ups covered a full glacial cycle (125 kyr) and used forcing suggested by SeaRISE [*Greve et al.*, 2011]. The north basin of IcIES is thinner and covers a smaller extent than the current ice sheet, while the south-west basin is thicker and more extensive than expected, due to the unconstrained freely evolving spin-up without tuning of the surface topography. SICOPOLIS' closer match to the present-day condition is due to a spin-up that after an initial relaxation run with freely evolving ice topography over 100 years that starts from the present-day geometry, proceeds with a full glacial spin-up that keeps the topography (surface, elevation, and ice margins) fixed to that of the relaxation run [*Greve et al.*, 2011]. PISM applies a flux correction to the surface mass balance in the final stage of the paleoclimatic spin-up to obtain an ice sheet geometry that is close to present day. Due to the expensive computing time associated with full-Stokes models, interglacial spin-ups are not practical with Elmer/Ice. However, in order to benefit from the long-term memory of the Greenland ice sheet evolution, Elmer/Ice's spin-up is initiated from SICOPOLIS' spin-up at 200 years B.P. via a two-step procedure. The topography of Elmer/Ice is first kept fixed for 100 years to allow fields to adjust from the shallow ice to the full-Stokes dynamics, followed by 100 years of topography relaxation to obtain the present-day configuration [*Seddik et al.*, 2012].

3. SeaRISE Experiments

[13] SeaRISE explores the sensitivity of ice sheets to imposed external forcing that aims to capture the response to changes in the atmospheric climate, basal conditions, and oceanic forcing. For the Greenland ice sheet, 10 simple perturbation experiments were designed and discussed in this section and in greater detail in *Bindschadler et al.* [2013]. Most models completed the full set of experiments, as illustrated in Table 1. Based on the response to these simple

forcings, SeaRISE designed a more complex experiment, with forcings chosen to represent the very high baseline emission scenario considered by the IPCC AR5. This experiment is, however, not considered in the present study. Although AIF performed more than one set of simulations, which differ in the sliding law for example, only one implementation is considered here, in order to prevent introducing bias in the spatial response.

3.1. Atmospheric Experiments (C1, C2, C3)

[14] The two forcings for the atmospheric experiments are anomalies in surface temperature and surface mass balance defined as the difference between precipitation and ablation. The temperature and precipitation data were calculated from a combination of the mean response to the A1B scenario from 18 climate models that participated in the Fourth Assessment Report (AR4; T. Bracegirdle, personal communication, 2009). The A1B scenario simulates rapid economic growth with energy from both fossil intensive and non-fossil sources [*IPCC*, 2007]. These IPCC simulations lasted 100 years and begin in
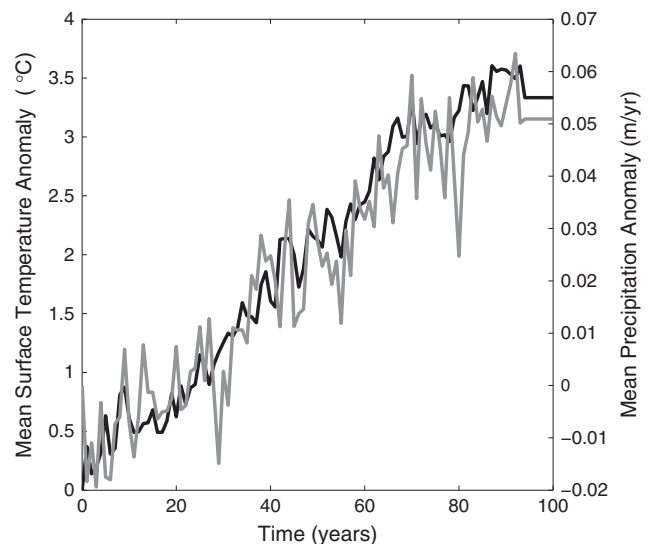

Figure 3. Surface temperature (black) and precipitation (gray) anomalies over the Greenland ice sheet corresponding to the IPCC AR4 A1B scenario, which forms the basis of the SeaRISE atmospheric scenarios.

calendar year 1998. The SeaRISE simulation begins 6 years later, in calendar year 2004, and lasts 500 years. The surface forcings for the SeaRISE atmospheric experiment thus varied for the first 94 years of the simulations and were held constant at the 94th year value thereafter. The temporal pattern of the A1B temperature and precipitation anomalies, averaged over the Greenland ice sheet is shown in Figure 3. The ablation was either obtained by a model's own positive degree day (PDD) scheme or from the SeaRISE data sets for the models that do not have a PDD scheme (see Table A1 in Appendix A). Three future atmospheric scenarios are considered by SeaRISE: The C1 experiment sets the temperature and precipitation anomalies to the A1B forcings, while the C2 experiment amplifies the A1B forcings by a factor of 1.5, and the C3 forcing prescribes anomalies that are twice as large as the A1B forcings.

3.2. Basal Sliding Experiments (S1, S2, S3)

[15] The enhanced sliding experiments are perturbation experiments that are designed to investigate the ice sheet response due to speeding up of the flow, implemented by prescribing an increase in sliding speed at the beginning of the simulations. Three amplifications of the basal velocities are considered: 2, 2.5, and 3 times for experiments S1, S2, and S3, respectively. The choice for the lowest amplification factor follows from the observed doubling in flow speed in Jakobshavn Isbrae in west Greenland and of the Helheim and Kangerdlugssuaq glaciers in south Greenland [*Joughin et al.*, 2004, 2008a, 2008b; *Stearns and Hamilton*, 2007]. The implementation of the experiment is model dependent due to the different sliding laws, and in particular, whether the boundary condition is imposed as a velocity or stress condition. In the first case, the forcing is implemented by amplifying the sliding coefficient, while the second case requires reducing the basal friction coefficient. Another difference in implementation of this experiment is due to mass-elevation feedback arising from the PDD capabilities in the surface mass balance schemes.

3.3. Ice Shelf Melting Experiments (M1, M2, M3)

[16] The potential effect of enhanced marine melt is explored by investigating the sensitivity of the ice sheet to basal melt rates at the ice-ocean boundaries. SeaRISE considers three melt rates: 2, 20, and 200 m/yr for experiments M1, M2, and M3, respectively. The largest melt rate is chosen to explore "high end" processes that erode margins. None of the ice sheet models participating in Greenland SeaRISE contain ice shelves, due to either the use of the shallow ice approximation that is only suitable for grounded ice sheet or to the fact that the reference elevation data [*Bamber et al.*, 2001a, 2001b] and land cover mask (Csatho, personal communication, 2009) do not contain ice shelves. The dynamic effect of ice shelves is however included in the UMISM model, by imposing a back stress on the grounded ice according to a theoretical formulation [*Thomas*, 1973] and a thinning rate at the grounding line according to *Weertman* [1974]. The experiment prescribes the melt rates at the grounding lines of the ice sheet, an implementation considered reasonable since melt rates are generally highest at the grounding lines [*Williams et al.*, 2001; *Payne et al.*, 2007]. The determination of the location of the ice-ocean boundaries or grounding lines is also model specific (see Table A1) and ranges from the last grounded grid point that is adjacent to

the ocean to where the ice thickness is at hydrostatic equilibrium. Grounding line migration is implemented with a flotation condition for all models that participate in the experiment, except for ISSM which does not allow its ice front to migrate. Once the ice front thickness of ISSM has melted away, melt rates are no longer prescribed, and changes are due to ice dynamics. As for the enhanced sliding suite of experiments, models that have PDD capabilities also include mass-elevation feedbacks.

3.4. Additional Scenarios

[17] The last experiment, C1S1, explores the sensitivity to multiple forcings by imposing simultaneously the atmospheric anomalies of 1x A1B (C1) and the 2x basal velocity amplification (S1). In order to mitigate the effect of different spin-ups, ice flow approximations, and model resolutions in the responses to the SeaRISE sensitivity experiments, models performed a constant climate control (CC) run that covered the same time period as their experiments. The philosophy is that any model transient resulting from the initial state or the representation of ice dynamics would influence control and sensitivity experiments in a similar fashion for that particular model. The resulting artifacts could therefore be removed by taking the difference between control and experiment. This concept was tested with a few models [e.g., *Greve et al.*, 2011] and indeed provided a means to filter out the artifacts of distinct spin-ups from the sensitivity to the SeaRISE experiment.

4. Basin Sensitivity to SeaRISE Experiments

[18] To explore the spatial response of the Greenland ice sheet to the SeaRISE experiments, the change in volume above flotation (ΔVAF) that occurs over seven basins after 100 simulated years is shown in Figure 4. For each model, ΔVAF is estimated via

$$\Delta\text{VAF} = \text{VAF}_{\text{exp}} - \text{VAF}_{\text{cc}} \qquad (1)$$

where VAF_{exp} is the VAF from an experiment and VAF_{cc} is the VAF from the control simulation. The VAF values are obtained from post-processing the SeaRISE submissions and are given by

$$\text{VAF} = A \times H_{\text{af}} \qquad (2)$$

where A is the grid area and H_{af} is the thickness above flotation.

[19] The ocean forcing experiments have the most diverse response in the change in VAF (Figure 4), where two types of behavior unfold: Models are either very sensitive to this forcing or little affected. The response to the climate and basal forcing is more homogenous, but the spread in response is larger for the sliding experiment than for the climate experiments. The C1S1 experiment, which imposes simultaneously the C1 climate and S1 enhanced basal lubrication, results in mass losses that correspond to the combination of these respective mass losses. *Bindschadler et al.* [2013] demonstrated this effect on a whole ice sheet basis; Figure 4 shows it occurs on a basin scale as well.

[20] In general, the response to an increased forcing is correlated with the response to the smallest applied forcing. For example, if a model experiences a mass loss as a result of the C1 climate experiment, it will also experience an increased mass loss with the more pronounced climatic forcing. The
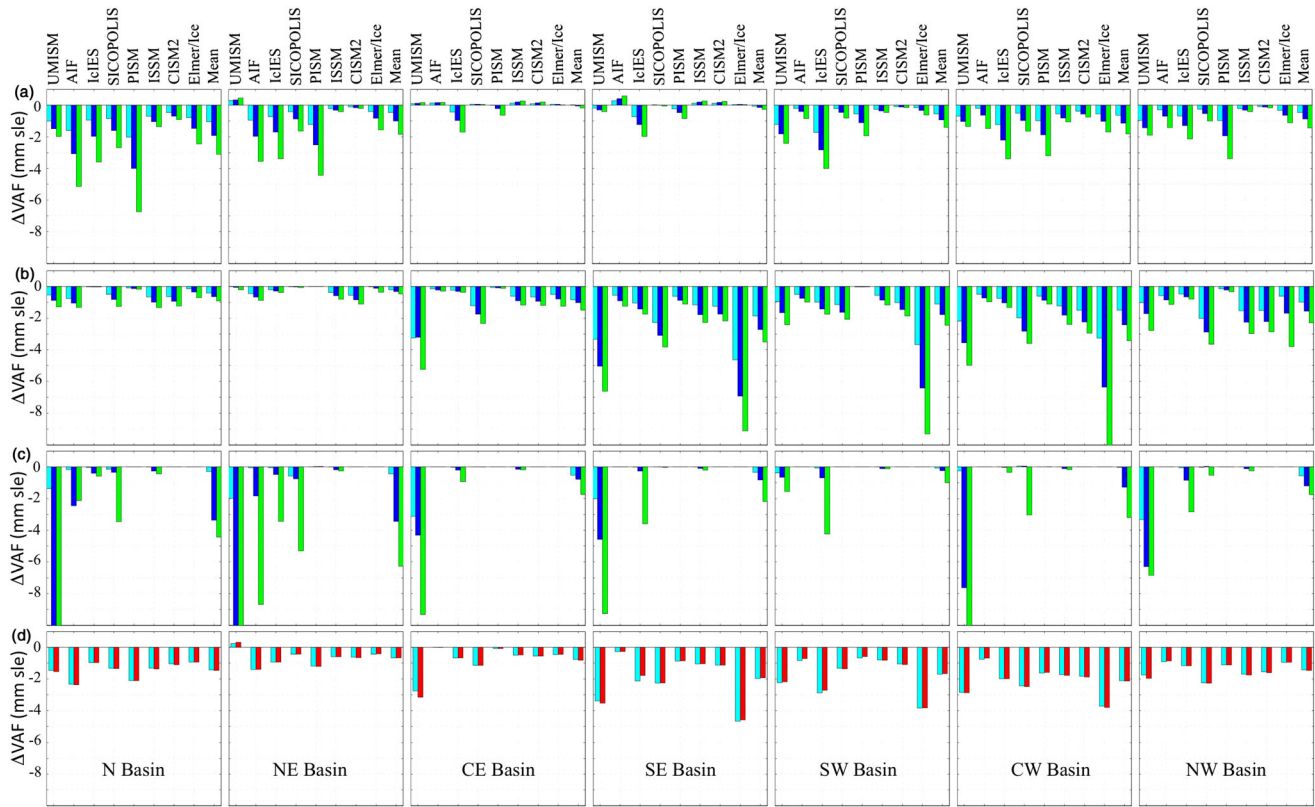
Figure 4. The change (experiment-control) in volume above flotation for the basins of the Greenland ice sheet (see Figure 1) after 100 simulated years. (a) Atmospheric forcings C1, C2, and C3 (light blue, blue, and green). (b) Sliding enhancements S1, S2, and S3 (light blue, blue, and green). (c) Melt rates M1, M2, and M3 (light blue, blue, and green). (d) Combination forcing S1C1 (light blue) and sum of C1 and S1 (red).

exception is PISM in the central east basin, where the C1 forcing results in a negligible mass gain that changes to a mass loss with the amplified C3 forcing. The response to the amplified melting experiments also results in an amplified mass loss. However, some models that are insensitive to the 2 m/yr and 20 m/yr melt rates lose mass with the 200 m/yr forcing (e.g., IcIES and SICOPOLIS in the north west basins). The larger oceanic forcing does in some cases lead to a mass loss that is equivalent to that from a smaller forcing (e.g., AIF in the north basin), indicating that the ice that is available for melt is already lost with the smaller melt rate. Thus, an increase in forcing is also associated with a larger dispersion in model response.

[21] Although Figure 4 illustrates the diversity in model response, there is no clear consistent outlier. A model that is extremely sensitive to the climate experiments will not be the most sensitive model to the enhanced sliding or oceanic forcing experiments. In addition, a model that is the most sensitive to a given experiment in one basin will not necessarily be the most sensitive in the other basins, nor will that basin remain sensitive throughout the other experiments for the given model. Furthermore, no model is always close to the ensemble mean behavior for the full set of experiments. The diversity in the modeled response is in part due to differences in (i) initial ice sheet configuration, (ii) ice flow dynamics and grid resolution, and (iii) implementation of the SeaRISE sensitivity experiments. For example, SICOPOLIS

and Elmer/Ice implement the climate sensitivity experiments using the same method [see *Seddik et al.*, 2012]. These two models differ in how they simulate ice dynamics: shallow ice versus full-Stokes and different mesh resolution (5 km structured grid versus 1 to 70 km anisotropic mesh). The fact that the change in VAF from these two models is similar for the climate sensitivities indicates that the mass loss is due to the change in surface mass balance and that the dynamic response does not play an important role nor lead to feedbacks on a 100 year timescale. In contrast, the distinct responses to the enhanced sliding experiment demonstrate the roles played by the dynamics, thermodynamics, and subsequent feedbacks in the ice sheet when dynamical forcing is introduced to models with different governing equations for the momentum balance.

[22] Despite the spread in responses to the SeaRISE forcings, trends do emerge and the resulting spatial behaviors are distinct for the four types of sensitivity experiments. This effect is most easily summarized by taking the average of all the models' ΔVAF for each experiment and basin. In the central eastern and south eastern basins, a number of models indicate a small growth with the climate experiments, but a few models also indicate a small mass loss such that the overall ensemble change is a negligible growth. The two regions that are the least sensitive are the north and north east for the sliding; the north east and the central east for the combination; and the south west and the central east basins for the imposed melt rate. The ensemble means indicate that the two regions
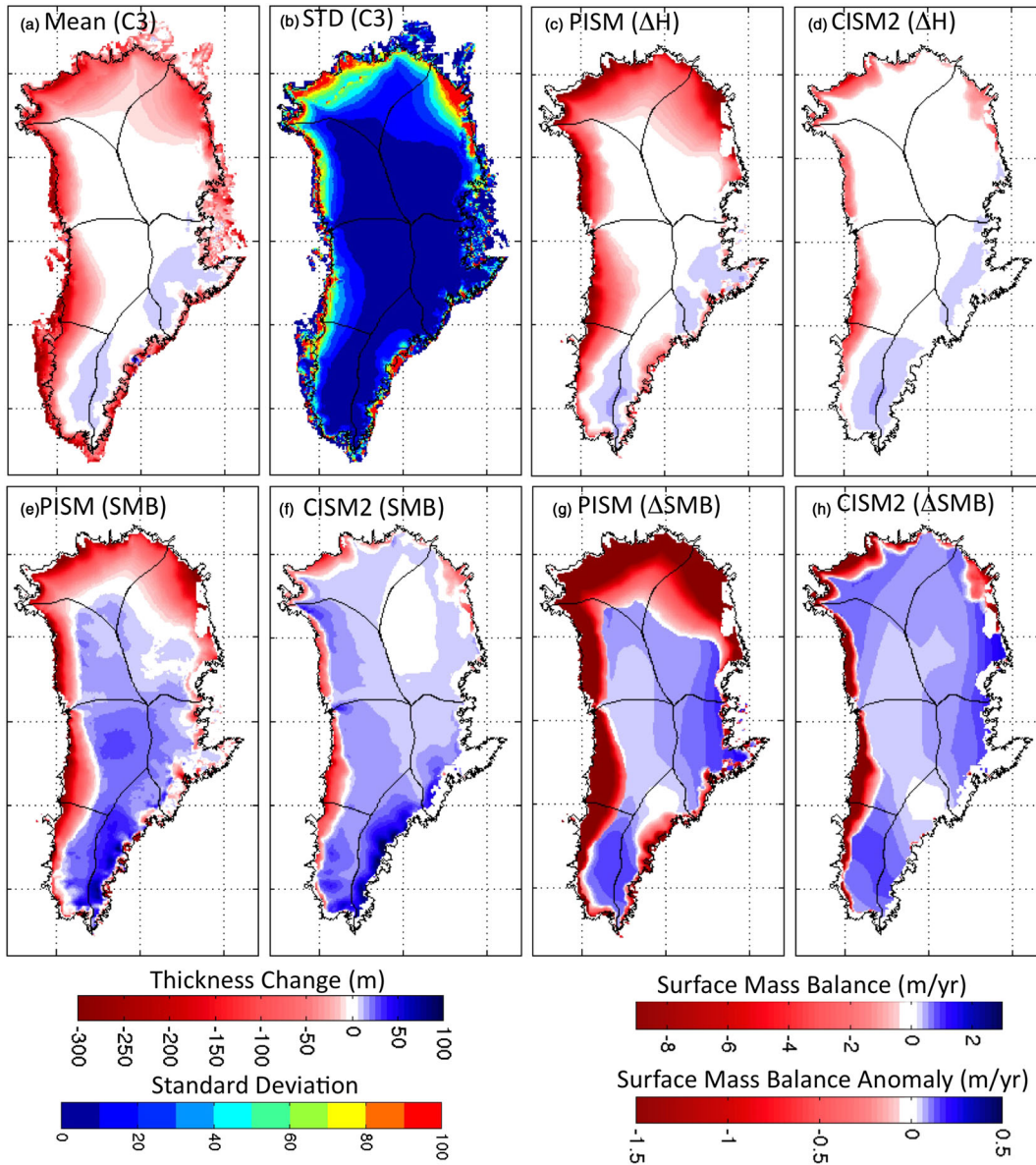
Figure 5. The ensemble mean thickness change from the (a) control and (b) standard deviation resulting from the C3 experiment after 100 simulated years, along with the thickness contribution from the (c) maximum (PISM) and (d) minimum (CISM2) models, and the surface forcings for these models: (e, f) surface mass balance and (g, h) surface mass balance anomaly at 100 years. The corresponding figures for all models are shown in the supporting information (Figures S1–S3).

that lose the most mass are the north and north east basins in the climatic set of experiments, the south east and central west basins for the enhanced sliding, the central west and south east basins for the combination experiment, and finally the north east and north basins for the oceanic forcing.

[23] The change in VAF on a basin-to-basin basis reveals important information on the spatial trends that emerge from the SeaRISE sensitivity experiments, but it does not provide insight as to whether the change in VAF is due to a change in thickness or in areal extent. Furthermore, it cannot address whether the ice response is uniform throughout a basin, or whether it is a localized effect. In addition, are the individual responses due to the different approximations of ice flow, the initial states, or to the implementation of the forcings? It is to

these types of questions that we now turn our attention. To focus our analysis, we choose to explore the resulting spatial patterns for experiments that yield similar ensemble change in VAF for the entire Greenland ice sheet (Table 1). We therefore illustrate the response to each type of SeaRISE sensitivity experiment by concentrating on C3, M2, S2, and C1S1, where each results in an ensemble volume change of approximately −10 cm sea level equivalent (SLE) over 100 years.

5. Spatial Response to the Atmospheric C3 Experiment

[24] The spatial response and sensitivity to a SeaRISE forcing is initially evaluated by comparing for each model the
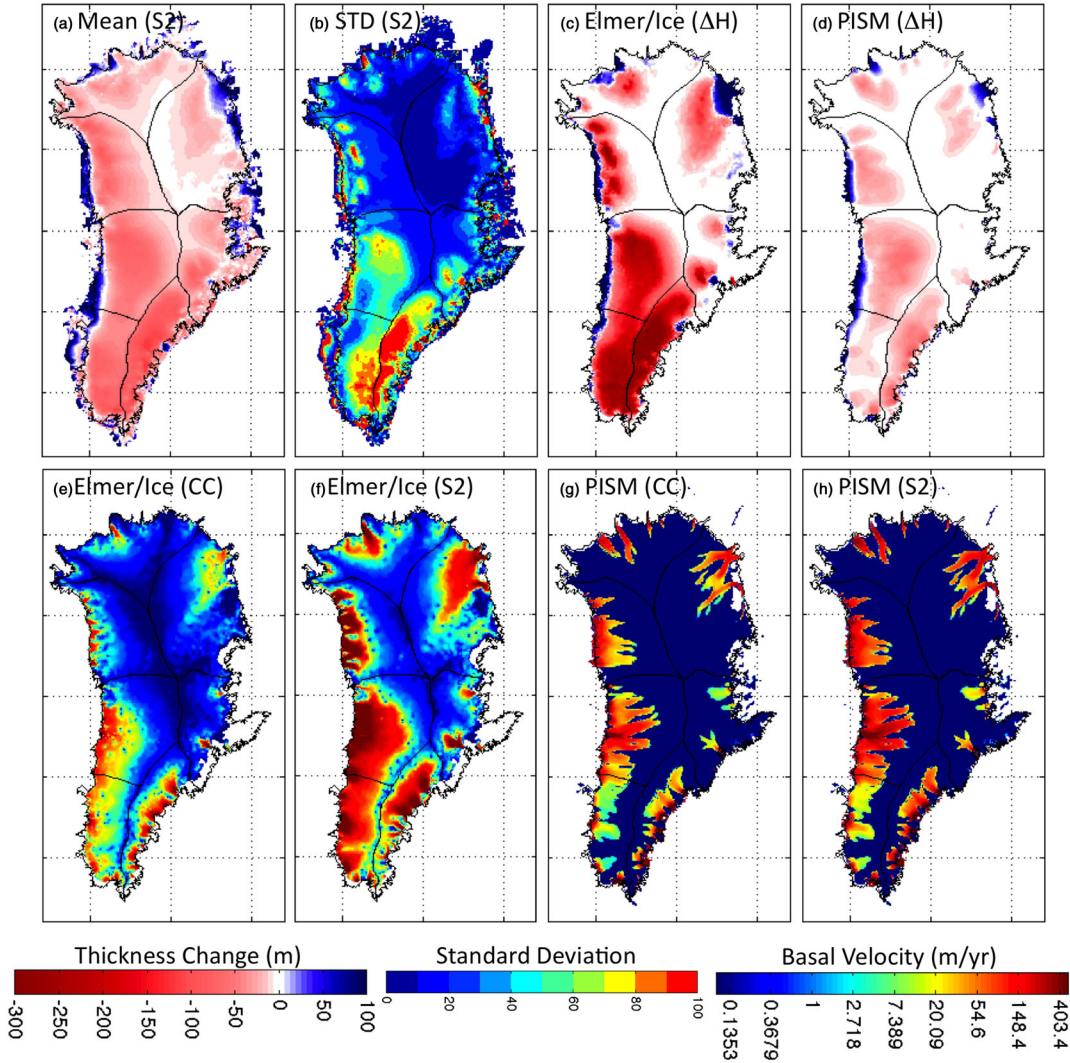
Figure 6. The ensemble mean thickness change from the (a) control and (b) standard deviation resulting from the S2 experiment after 100 simulated years, along with the thickness contribution from the (c) maximum (Elmer/Ice) and (d) minimum (PISM) models. The basal velocity at 100 years from the control and S2 experiments for (e, f) Elmer/Ice and (g, h) PISM. The corresponding figures for all models are shown in the supporting information (Figures S4–S6).

change in thickness between an experiment and the control simulation, given by

$$\Delta H = H_{\exp} - H_{cc} \qquad (3)$$

where $H_{\exp}$ and H_{cc} are the thickness of the experiment and control after 100 years of simulation. The individual model's change in thickness is then combined to form the unweighted ensemble mean and standard deviation, following the IPCC "one model, one vote" approach [*IPCC*, 2007; *Knutti et al.*, 2010a].

[25] The C3 experiment, which considers an amplification of the A1B forcing by a factor of 2, leads to a small growth over the interior of the south east, south west, and central east basins, and all basins display a large thinning at the margin of the ice sheet compared to the control after 100 years (Figure 5a). The low standard deviation for the ensemble of the models throughout most of the ice sheet in Figure 5b indicates that the individual modeled responses are close to

the ensemble mean. The spread in model responses for this atmospheric forcing is confined to the periphery of the ice sheets, as reflected by the high values of standard deviations throughout the marginal areas. The model that is the most sensitive to this forcing, PISM with a change in VAF of −21.14 cm SLE (Table 1 and Figure 5c), displays a thickness response that correlates well with the ensemble behavior. In contrast, the least sensitive model, CISM2 with a change in VAF of −1.68 cm SLE (Table 1 and Figure 5d), experiences extensive growth in the south of the ice sheet and a negligible change in the north and north east basins, where the ensemble behavior indicated a moderate thinning.

[26] The implementation of this experiment was not uniform because the ablation scheme used by the models varied: PISM computed its own ablation, while CISM2 applied the forcings provided by SeaRISE. The resulting surface mass balances (Figures 5e and 5f) are therefore distinct, due to different initial surface mass balances and in particular to distinct surface mass balance anomalies (Figures 5g and 5h).

These anomalies can vary between models due to PDD schemes that use surface temperatures, which are for most models parameterized to depend on surface elevation following *Fausto et al.* [2009]. Positive feedback can therefore be established, as lower elevations are exposed to warmer temperatures and thus increased ablation. The surface mass balance anomaly used by CISM2 is positive over most of the ice sheet, with the largest contribution in the south east basin. The negative surface mass balance anomaly is confined to a narrow band that follows the northern and western margins of the ice sheet. PISM's surface mass balance anomaly is also positive in much of the interior of the ice sheet and largest in the south east basin, but the negative surface mass balance anomaly extends further inland than for CISM2 (for example, over half of the north and north eastern basins experience a negative surface mass balance anomaly). Furthermore, PISM's negative surface mass balance anomaly is generally larger than for CISM2.

[27] With both PISM and CISM2, the patterns of thickness change are highly correlated with the surface mass balance anomaly, suggesting that the spread in model responses in Figure 4 arises predominantly due to the different surface mass balance anomalies (which are related to the initial conditions and PDD schemes), and not caused by the ice flow dynamics. The only two models with no PDD schemes, ISSM and CISM2, have similar spatial (Figure 4) and temporal [*Bindschadler et al.*, 2013] responses to the climate forcings and are the least sensitive of the ensemble. In contrast, models with PDD schemes are more sensitive to the climate experiments due to the ice elevation/surface mass balance feedbacks and the different PDD schemes result in a greater spread in surface mass balance anomalies and ice sheet responses. However, when the PDD schemes are the same, which is the case for SICOPOLIS and Elmer/Ice [*Seddik et al.*, 2012], the spatial and temporal responses to the climate forcings are comparable (see supporting information and *Bindschadler et al.* [2013]).

6. Spatial Response to the Basal Sliding S2 Experiment

[28] The ensemble behaviors that emerge after 100 years of simulation from the ice thickness response to the S2 forcing (a sliding enhancement by a factor of 2.5 at the beginning of the simulation) include a thickening of the periphery, a small thinning over the interior of the north, north east, and north west basins, and pronounced thinning in the interior of the central west, central east, south west, and south east basins in Figure 6. The standard deviation for the ensemble is low throughout much of the deep interior of the three north basins. The spread in model responses for the northern basins is confined to isolated "hot spots" that correspond to the fast flowing outlet glaciers such as Humboldt and Petermann in the north basin. The most striking feature, however, is the significant standard deviation in the interior of the south west, south east, and central east basins, which indicates considerable scatter in the response to the S2 experiment. This dispersion was already apparent in Figure 4 with Elmer/Ice, UMISM, and SICOPOLIS contributing the most to the ensemble mean after 100 years. The standard deviation map indicates that the variation in thicknesses occurs throughout the entire basins.

[29] Further insight into the distinct behaviors is gained by looking at the two extreme cases, namely, PISM and Elmer/Ice which contribute to a mass loss of −2.18 cm SLE and −22.65 cm SLE, respectively (Table 1). The enhanced basal velocities lead to an increased flow of interior ice, such that both models experience a thickening of the margins at the outlet of the fast flowing ice streams and a thinning over the interior of the basins (Figures 6c and 6d). The interior thinning is uniform for PISM, except over the central west and south east basins. Elmer/Ice's interior thinning varies in spatial extent and magnitude and clearly dominates the signal of the ensemble mean.

[30] These models differ in the physics used to solve for the ice motion, their spatial resolution, and the sliding laws: PISM uses a nearly plastic sliding law [*Schoof and Hindmarsh*, 2010], while Elmer/Ice implements a temperature dependent Weertman sliding law. For both models, however, the determination of areas that are experiencing basal sliding is a complex process that involves thermal and dynamical feedbacks. The basal slipperiness at the beginning of any simulation is a result of the spin-up, and therefore the location of the regions of where the enhanced sliding occurs in the S2 experiment differs in the two models. In addition, since the ice sheets of experiment S2 evolve differently from those of the control simulations, different basal stresses and temperatures emerge, such that the ratio of experiment to control basal velocities will not remain constant in time. Nonetheless, comparing the spatial patterns of the basal velocities in the control and S2 simulations at 100 years provides insight into the different sensitivities of the PISM and Elmer/Ice models to the sliding experiment. The regions that are experiencing faster basal flow in the PISM S2 simulations (Figure 6h) are restricted to the regions that were already fast flowing in the control simulations (Figure 6g), due to the sharp frozen-thawed boundaries in PISM's basal velocities. In contrast, the gradual decay of basal slipperiness in the Elmer/Ice's simulations results in basal sliding that extends further into the interior of the ice sheet, and thus a larger portion of the ice sheet is subjected to the enhanced flow experiment in the Elmer/Ice simulations (Figures 6e and 6f) compared to the PISM simulations.

7. Spatial Response to the Ice Shelf Melting M2 Experiment

[31] The response to the M2 oceanic forcing (melt rate of 20 m/yr) is presented in Figure 7. Localized small thickening occurs on the periphery of the ice sheet; however, the dominant pattern of the ensemble mean in Figure 7a is the large thinning over the outlet glaciers which propagates inland, with the exception of the central east and south west basins. The large standard deviation reflects the range of thinning magnitude experienced by the different models. Indeed, the change in basin VAF (Figure 4) indicates that this set of experiment resulted in the most heterogeneous response.

[32] None of the models taking part in the Greenland suite of experiment include ice shelves as indicated in Table A1. UMISM is the most sensitive model to the melting experiments with a mass loss of −57.48 cm SLE after 100 years of simulation (Table 1). Its grounding line position is determined by the location where the surface drops below flotation height, and the effects of ice shelves are approximately
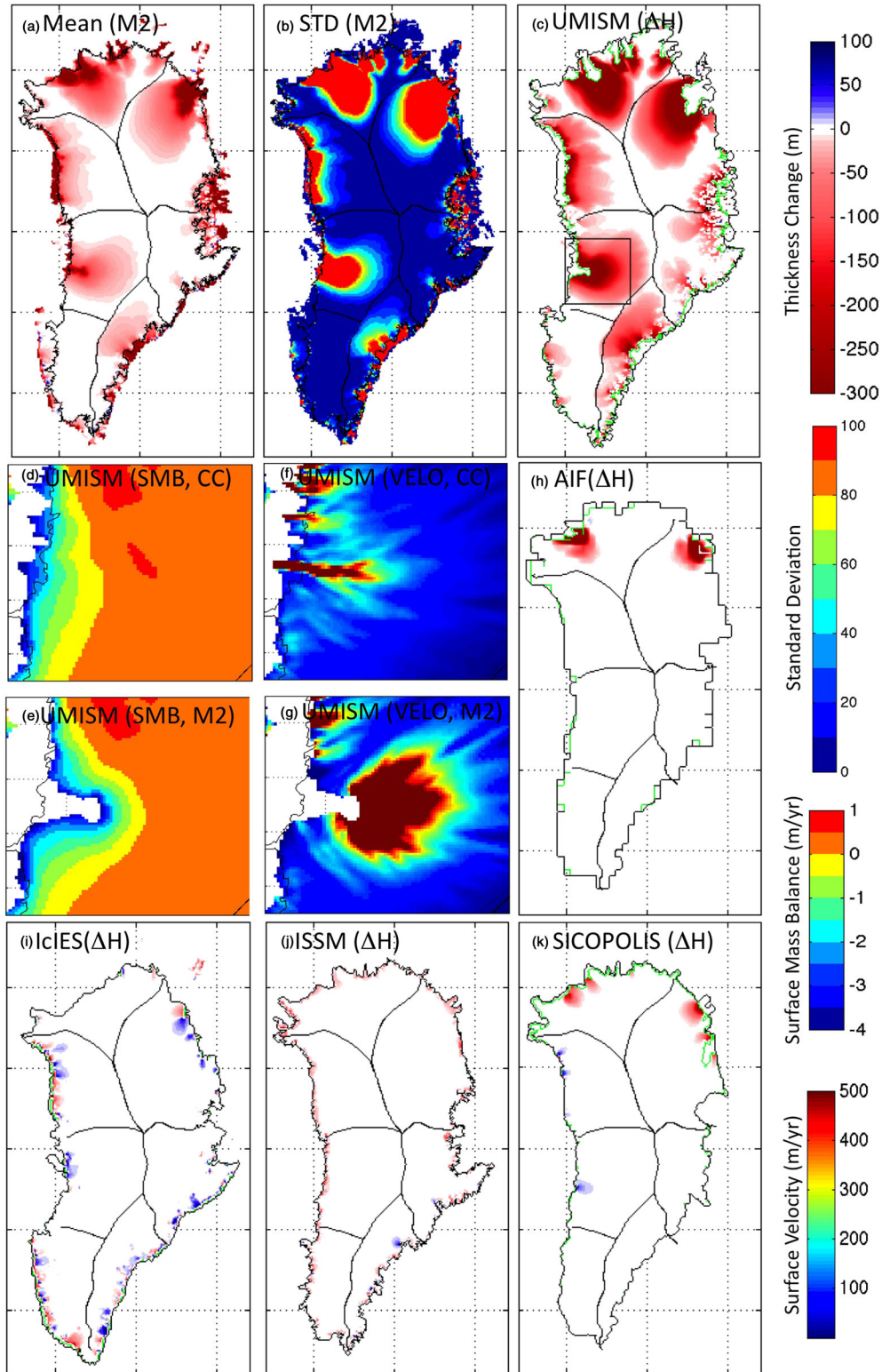
Figure 7. The ensemble mean thickness change from the (a) control and (b) standard deviation resulting from the M2 experiment after 100 simulated years, along with the thickness contribution from the (c) maximum model (UMISM). (d and e) UMISM control and M2 surface mass balances and (f and g) surface velocities at 100 years. The thickness change associated to (h) AIF (i) IcIES,(j) ISSM, and (k) SICOPOLIS after 100 years. The grounding line for the M2 experiment at 0 and 100 years is shown in black and green.
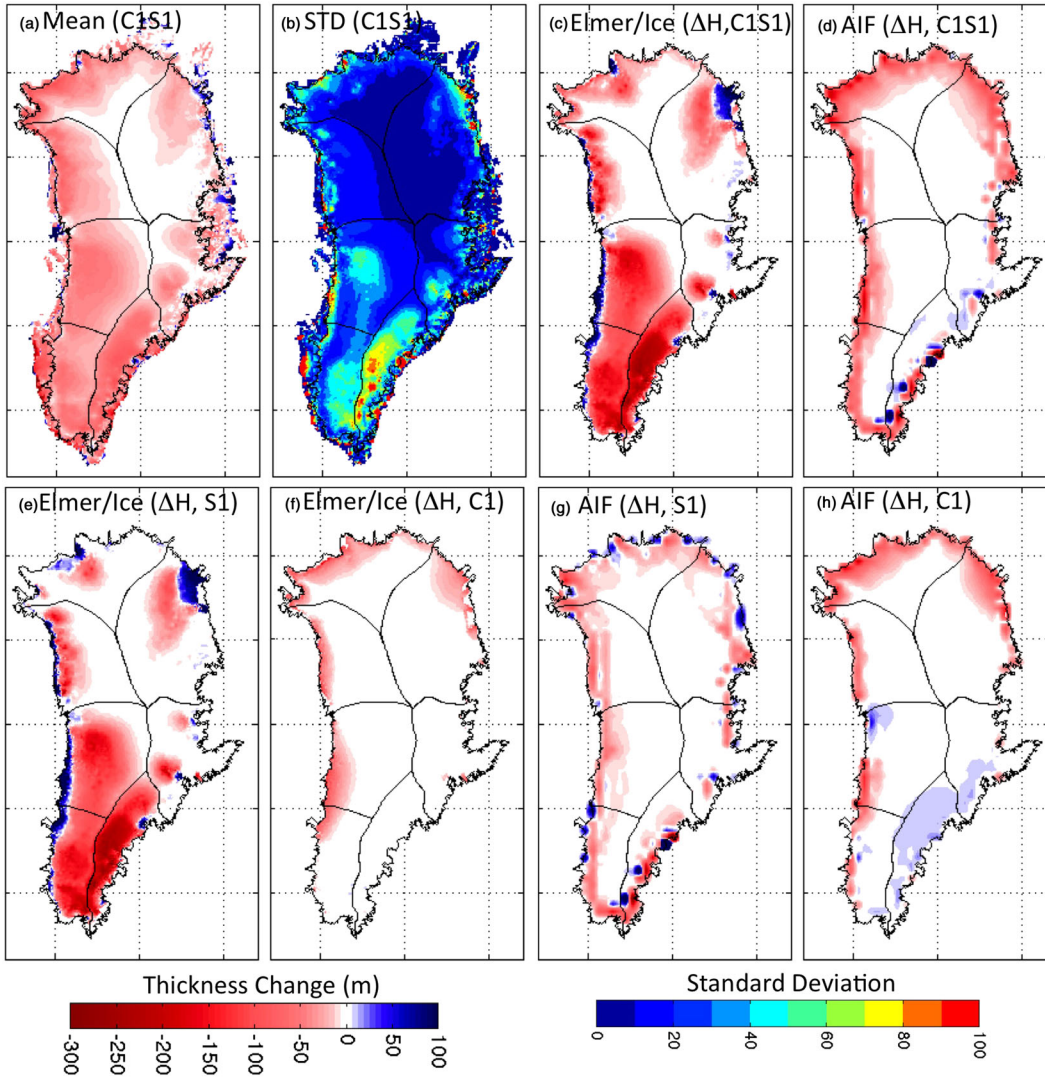
Figure 8. The ensemble mean thickness change from the (a) control and (b) standard deviation resulting from the C1S1 experiment after 100 simulated years, along with the thickness contribution from the (c) maximum (Elmer/Ice) and (d) minimum (AIF) models, and the thickness change due to the S1 and C1 experiments for (e, f) Elmer/Ice and (g, h) AIF. The corresponding figures for all models are shown in the supporting information (Figures S7–S9).

introduced by imposing at the grounding line an ice shelf spreading rate [*Weertman*, 1974] and ice shelf back stress [*Thomas*, 1973]. The ocean melting is applied at the grounding line, and the result is a grounding line retreat of the marine terminating outlet glaciers accompanied by a thinning wave that propagates inland in Figure 8c. A positive feedback is established, as the lower surface elevation is then exposed to warmer air temperatures that result from the elevation-dependent temperature scheme [*Fausto et al.*, 2009] and thus experience increased surface melting. Thus, areas in the vicinity of the new ice front of Jakobshavn Isbrae experience a negative surface mass balance with the M2 simulation that was formerly positive with the control run, as illustrated in Figures 7d and 7e. Together, these processes affect the flow pattern of the ice sheet as reflected by the surface velocity (Figures 7f and 7g). For example, an increase in surface velocity is observed at the new calving front of Jakobshavn Isbrae and over most of the basin. The

outlet glaciers that were adjacent to the old trunk of Jakobshavn Isbrae have diverted their flow, such that the ice that once fed these areas is now being drawn into the faster-flowing main channel.

[33] As the M2 experiment results in the most diverse response (Figure 4 and Table 1), the thickness change of the remaining models that participated in the experiment is also shown in Figure 8. The mass losses from AIF, IcIES, ISSM, and SICOPOLIS are -4.29, -2.90, -1.02, and -1.01 cm SLE, respectively, and the patterns of thickness change are related to the location of where the melt rates are prescribed. ISSM applied the melt rates where the ice front of a marine terminating glacier is at hydrostatic equilibrium and the bed below sea level. As the grounding line of ISSM does not migrate, the melting stops when the marine ice front has melted away. Thinning therefore occurs at the front of the outlet glaciers and is confined to the periphery of the ice sheet. The models AIF, IcIES, and SICOPOLIS

allow their grounding lines to migrate, based on the hydrostatic equilibrium condition, but unlike in UMISM, the longitudinal stress transfer from ice shelves is not approximated at the grounding line in these models. In the north and north east basins, AIF and SICOPOLIS experience a grounding line retreat and interior drawdown that is similar to UMISM in Figure 7, but that does not extend as far inland. The ice sheet that results from IcIES' spin-up covers a smaller spatial extent in the north basin than the current ice sheet (see Figures 1 and 2) and thus does not include the ice streams that could drain the ice sheet (e.g., Petermann or Humboldt), explaining the negligible change in VAF in this basin (Figures 4 and 7i). IcIES does, however, capture the inland thinning associated with Nioghalvfjerdsbrae in the North East basin, but the adjacent ice also experiences a thickening, indicating that the flow patterns have changed. In light of the behaviors of AIF, SICOPOLIS, and IcIES in the north basin, their negligible response and grounding line retreat in the vicinity of Jakobshavn Isbrae are unexpected. Our explanation for these behaviors is the coarse grids used by the models (10 km for SICOPOLIS, 40 km for AIF, and 10 km for IcIES) compared to the size of the channel and the use of non-ice-shelf models without special parameterization of the ice shelf stresses at the grounding line.

8. Spatial Response to the Combination C1S1 Experiment

[34] The combination experiment, C1S1, imposes simultaneously the AR4 climate forcing and the doubling of the basal lubrication. This combination experiment results in a mass loss that is comparable to the sum of the C1 and S1 forcings (Table 1). The thickness change pattern for this forcing, shown in Figure 8a, resembles the superposition of the distinct responses to the atmospheric and enhanced sliding sensitivities. The pronounced thinning that was characteristic of the S2 forcing over southern Greenland remains present in C1S1, but is now less severe due to growth associated with the climate forcing. The outward thickening of the periphery resulting from S2 is dominated by the strong thinning associated with the climate, such that the periphery experiences a mass loss, except over a few isolated spots located predominantly in the north east basin. The standard deviation pattern in Figure 8b is also a combination of the qualitative behaviors from the standard deviation of the climate and sliding forcing, but results in lower values than the individual standard deviations shown for the C3 and S2 experiments. This is due to the lower spread in response for the C1 and S1 experiments compared to their respective amplified forcings (see section 4).

[35] As with the S2 experiment, the full-Stokes model Elmer/Ice is the most sensitive model to the C1S1 forcing and produces a mass loss of −15.10 cm SLE. AIF is the least sensitive model, contributing −6.49 cm SLE. In addition to the changes in ice thickness from the C1S1 experiment for Elmer/Ice and AIF, results from the individual S1 and C1 forcings are also shown in Figure 8. Elmer/Ice's interior thinning with the C1S1 forcing is characteristic of its response to the enhanced sliding, indicating the high sensitivity of this model to the basal forcing. The climatic forcing does, however, play a small role and results in thickening along the ice divides of the north, north west, north east, central west,

and central east basins. The peripheral thinning experienced by Elmer/Ice due to the negative surface mass balance dominates the peripheral growth due to S1 in the north basin, but is not sufficient to balance the S1 peripheral thickening in the central west and south west basins. In contrast, the C1S1 interior response from AIF is dominated by the C1 forcing. The peripheral thinning along the western and northern margins due to the climate forcing is either enhanced by the thinning arising from the S1 forcing or dominates the S1 thickening, such that these regions now experience thinning. Along the south east and central east margins, however, the S1 response dominates the C1S1 signal. Furthermore, the interior climatic growth of the central east basin offsets the peripheral thinning due to the enhanced sliding, such that the overall change in VAF in this basin is negligible (see also Figure 4).

[36] For all models, the increased flow of ice, due to the amplified basal slipperiness, to the margins of the ice sheet, where the surface mass balance is negative, results in a mass loss that is greater than that from the individual forcings: When atmospheric or sliding forcings are considered on their own, a larger amplification of the individual forcings is required in order to obtain a mass loss that is comparable to the combination forcing. Indeed, Table 1 shows that C1S1 results in a mass loss of 9.99 cm SLE, which requires the C3 or the S2 amplifications to obtain similar mass losses (10.06 and 10.29 cm SLE, respectively).

9. Temporal Evolution After 200 Years

[37] After 100 years of simulations, the mass loss due to the C3, M2, S2, and C1S1 sensitivity experiments was similar and of order −10 cm SLE for the ensemble mean, but this is no longer the case at 200 years. As shown in *Bindschadler et al.* [2013], the time evolution of the change in volume for these four sensitivity experiments is not homogeneous: The initially slow response to the climate forcing accelerates in time, while the instantaneous rapid decay associated with the oceanic and basal forcings later decelerates. At 200 years into the simulations, the change in volume above flotation is now −25, −19, −16, and −13 cm SLE, respectively, for the C3, C1S1, S2, and M2 experiments. The ice sheet therefore adjusts at different rates to the different external forcings, and how this is reflected in the thickness response is the focus of this section.

[38] The climatic forcing, C3, results in the largest mass loss from the Greenland ice sheet with a threefold increase in change in VAF compared to the mass loss at 100 years. As explained in the experimental setup, the surface forcings are kept fixed to their 94th year value and are thus similar to the ones presented in section 3, with differences arising from elevation feedbacks in the surface temperature and ablation for the models that have PDD schemes. The mean thickness change (Figure 9a) displays similar characteristics as its earlier response, namely, an interior growth due to the positive surface mass balance in this region. The spatial extent of the thickening is reduced in all basins, except for the central east and north east basins. The thinning over the ice front caused by the negative surface mass balance intensifies and propagates inland into regions of positive surface mass balance, indicating a dynamical response from the ice sheet that is driven by processes at the margins. The standard deviation remains low over the interior, but the high peripheral
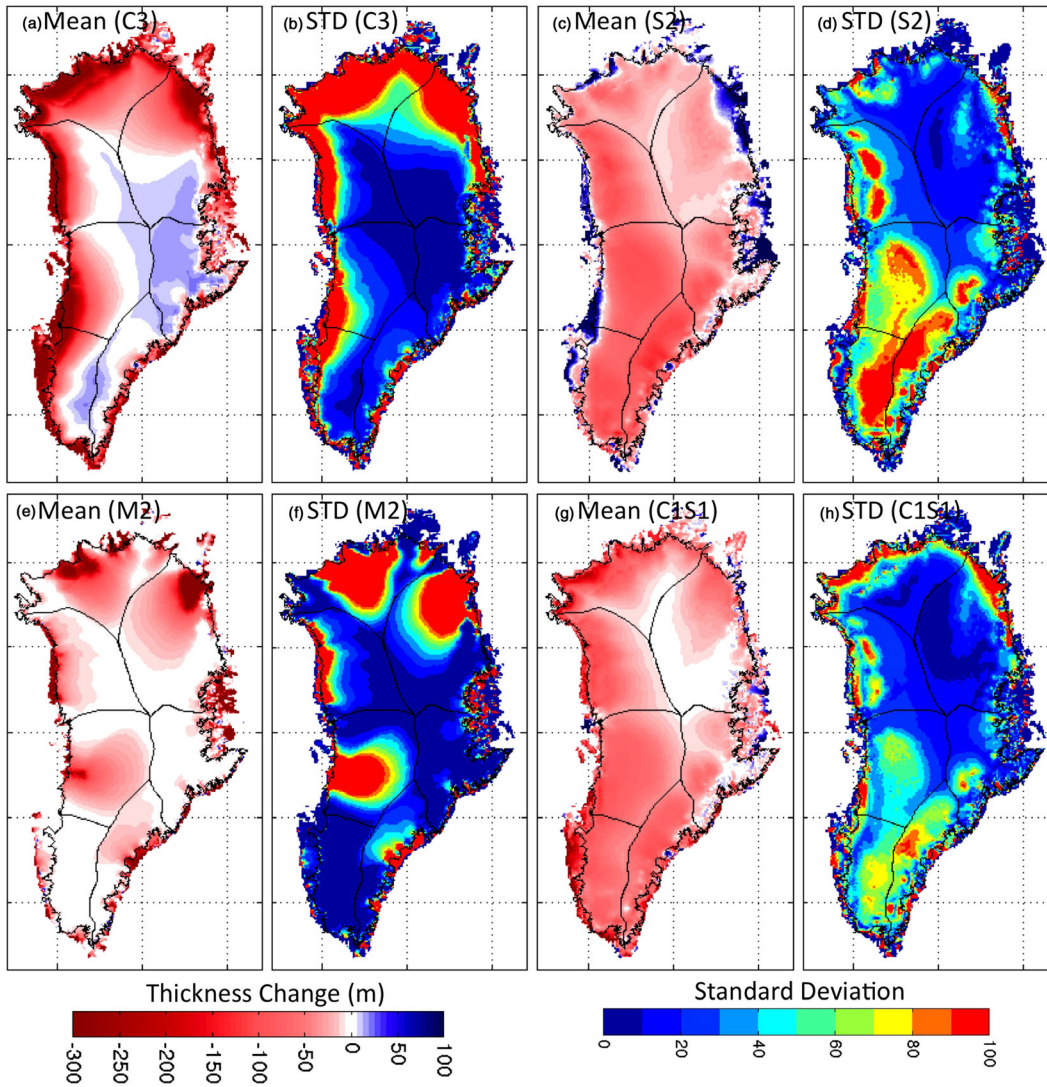
Figure 9. The ensemble mean thickness change from the control and standard deviation after 200 simulated years resulting from the (a, b) C3 experiment, the (c, d) S2 forcing, the (e, f) M2 forcing, and the (g, h) C1S1 experiment. The thickness change for all models is shown in the supporting information (Figures S10–S13).

values reflect a spread in model responses. The shallow ice model SICOPOLIS and the full-Stokes model Elmer/Ice, which implement the forcings identically, continue to lose a comparable ice volume (−20.30 and −19.94 cm SLE, respectively, see *Bindschadler et al.* [2013]), suggesting that the diversity in responses therefore continues to be predominantly due to differences among the various schemes for implementing surface mass balance (SMB) (e.g., PDD versus the SMB provided by SeaRISE). This effect is particularly noticeable in the high standard deviations in the northern basins that are correlated to regions in Figures 5e and 5f where the negative surface mass balance of the most sensitive model (PISM) extends farther inland than for the least sensitive model (CISM2).

[39] The peripheral growth and interior drawdown from the increased outward flow of inland ice associated with the enhanced basal sliding sensitivity experiment S2 continue to be the characteristic response after 200 years of simulation (Figure 9c). The ice front thickening along the western margins does not however extend as far inland as it used to. The different thickness changes in the near margins after

200 years compared to those after 100 years reflect the dynamic adjustment of the system to the initial perturbation in basal velocities. The prescribed increase in basal velocities leads to an ice flow speedup that transports mass from the interior to the margins, which results in a thickening or advancing of the ice front and a thinning of the interior. With time, the ice sheet surface adjusts to the new basal conditions and surface elevation feedback starts to dominate: Increased ablation in the near margins results in the thinning of the periphery seen after 200 years of simulation, for example. Adjustment of the ice sheet surface is expected to continue until the ice sheet geometry is again in balance with its mass input.

[40] The M2 sensitivity experiment has now become the least sensitive forcing, but also remains the experiment with the most diverse response [*Bindschadler et al.*, 2013]. The only true contributor to the thickness response shown in Figure 9e continues to be UMISM, and thus the response to the oceanic forcing is potentially underestimated. The retreat of UMISM's outlet glaciers has either slowed down or stopped (due to the grounding line having stopped its retreat),

but the inland drawdown continues. In particular, the thinning wave caused by Jakobshavn Isbrae nearly reaches the basin divide, illustrating the potential for outlet glaciers to rapidly drain their basin catchments as a response to warmer oceanic conditions and associated atmospheric positive feedbacks.

[41] The C1S1 forcing produces a doubling in mass loss compared to its effect after 100 years. The pattern of thickness change in Figure 9e continues to be a combination of the respective responses to the climatic and enhanced sliding signals. In particular, the peripheral thinning from the warmer atmospheric conditions and the interior drawdown due to the increased basal sliding over the western and southern basins remain the dominant responses. In the north and north east basins, the negative surface mass balance leads to a peripheral thinning that propagates farther inland. By 200 years, the resulting marginal thinning is greater than marginal thickening arising from increased outflow of inland ice due to basal lubrication. Furthermore, this peripheral imbalance is accentuated as the ice sheet continues to thin and flatten, thereby reducing the local driving stress and outflow. In the central east basin, the thickening from the positive surface mass balance alleviates the thinning from the basal forcing.

[42] The spatial evolution continues in time along the same trends shown in this section. We do not investigate the spatial patterns at later times, because two out of the eight models participating in SeaRISE stopped their simulations (CISM2 and Elmer/Ice) at 200 years, due to the computational costs associated with higher-order models.

10. Discussion and Conclusion

[43] SeaRISE explored the effect of changing oceanic conditions, a warmer atmospheric environment, and its associated effect in increased surface melt water that could reach the base of ice sheets. The analysis presented here focuses on the spatial response of the Greenland ice sheet thickness after 100 years and 200 years of simulations. This choice of time is motivated by the fact that it includes the maximum number of participating ice sheet models, but more importantly because the ensemble mean mass loss from three distinct SeaRISE forcings (C3, S2, and M2) and the combination of S1C1 leads to an ensemble mean mass loss that is comparable and of order −10 cm SLE after 100 years of simulations, but to disparate mass loss at other times [*Bindschadler et al.*, 2013].

[44] The individual model responses to the SeaRISE sensitivity experiments are distinct due to their particular implementations of the external forcing, their respective approximation of ice flow dynamics, spatial resolutions, sliding laws, treatment of the grounding line, and initialization procedures. For example, external feedbacks are introduced in the enhanced sliding experiments, as a change in thickness will result in a change in surface temperature and thus surface mass balance for models that have PDD schemes. As no model is consistently the outlier in all of the experiments, the impact of model physics and spin-up on the projection was explored with an unweighted ensemble analysis. There is, however, no guarantee that the response of the ensemble mean is more likely or accurate than any of the individual responses [*Knutti et al.*, 2010b], but this approach allows an initial estimate of sensitivity to parameter change to be evaluated as broadly as possible. General trends that are consistent in all

models do emerge, and distinct responses to the different types of sensitivity experiments are seen in the model ensemble, such that the geographical change in thickness displays a characteristic signature depending on the applied forcing.

[45] The basin-to-basin analysis reveals that although some experiments result in a similar total mass loss, the sectors that are vulnerable to the external forcings differ with each type of sensitivity experiment. Furthermore, an amplified volume loss in these basins results with an increase in forcing. The north and north east basins are the most sensitive to the oceanic and atmospheric forcings, while the south east and central west basins respond the most to the enhanced sliding and the combination experiment. The geographical patterns of thickness change further illustrate that the complex basin response originates from either the ice front, the outlet glaciers, or the interior of the ice sheet. With time, the thickness change propagates at different rates, and to specific regions, depending on the sensitivity experiment.

[46] The spatial response to the climate forcing that was implemented via anomalies in surface mass balance and temperature leads to an interior growth of the ice sheet and a thinning of the periphery. The pattern is highly correlated to the imposed surface mass balance anomaly, namely, thinning/ thickening occurs over regions of negative/positive surface mass balance anomaly. This experiment results in the most homogeneous model response, and when both the initial volume of the ice sheet and the imposed forcings are similar, the response of shallow ice models is comparable to that of a full-Stokes model as demonstrated by SICOPOLIS and Elmer/Ice. These behaviors therefore suggest that on a 100–200 year timescale, the effect of changes in surface mass balance can be examined with the current generation of ice sheet models and does not create significant dynamic response.

[47] Although the future A1B precipitation anomalies were the same for all models, the ablation anomalies were model specific, such that the actual surface forcing applied to the ice sheet differed for each model. The set of models that were the most sensitive to this forcing applied their own PDD schemes to infer ablation. The amount of melt in turn depends on the surface temperature which in most cases varied with elevation following *Fausto et al.* [2009], allowing feedbacks to be established. In contrast, the least sensitive models did not have PDD schemes, and thus imposed as anomalies the temperature and surface mass balance provided by SeaRISE, which were produced by the A1B climate model ensemble. In addition, the models with PDD schemes initialized using interglacial spin-up and, as a result, were generally thicker than the present-day ice sheet. The models with no PDD schemes used initialization methods based on data assimilation of present-day conditions. This distinction suggests that the mass loss due to atmospheric forcing is highly sensitive to the initial ice volume and ice sheet configuration, indicating that quantification of future sea level evolution requires careful initialization.

[48] The potential changes in the magnitude and extent of basal sliding lead to thickening at the edge of the ice sheet and inland thinning resulting from the increased flow of inland ice. Model sensitivities can be traced back to the choice of sliding law and the determination of the basal slipperiness beneath the ice sheet. Furthermore, the spatial resolution of the models influences their capability of simulating the narrow fast-flowing outlet glaciers. The most diverse thickness

change occurs in southern Greenland, a region where the basal topography is poorly known. It is hoped that as our knowledge of the basal topography increases and its associated uncertainty reduces, the modeled ice sheet responses in this region will converge.

[49] The experiment that combines the C1 atmospheric forcing to the S1 flow enhancement aims to investigate the response of simultaneous warmer atmospheric conditions and speed up of the flow. The thickness response to the C1S1 forcing is a combination of the individual changes observed with the S1 and C1 forcing: when the magnitude of the thickness change from the sliding exceeds the opposite response due to the climatic forcing, the thickness change resembles the response to the enhanced sliding experiment and vice versa. As the basal sliding increases the flow of ice to regions of negative surface mass balance at the edge of the ice sheet, the mass loss from the combination experiment exceeds the mass loss due to the individual forcing. A mass loss that is comparable to the C1S1 forcing after 100 years of simulations can only be obtained with the amplified atmospheric forcing C3, or with the S2 sliding experiment. Thus, without the inclusion of processes associated with atmospheric warming that have the potential for additional water to reach the base of the ice sheet (for example increased production of surface meltwater [*Zwally et al.*, 2002; *Parizek and Alley*, 2004; *van de Wal et al.*, 2008; *Das et al.*, 2008] or rain [*Howat et al.*, 2008]), predictions of future sea level will be underestimated. However, increased amount of basal water could also create a better hydrologic network under the ice, allowing water to be more easily evacuated, resulting in glacier slowdown rather than speedup [*Schoof*, 2010]. It is therefore crucial to understand how surface melt water affects the basal hydrology and basal sliding, along with the development of parameterizations that (i) capture these processes and (ii) can be implemented in whole ice sheet models.

[50] The greatest spread in model response is associated with the oceanic sensitivity experiments, as models are either extremely sensitive to this forcing or not at all. The conflicting responses are due to the different implementation of the forcing and the parameterization of marine terminus evolution and spatial resolution. The coarse-grid resolution of the models, which is often comparable to the width of many of the outlet glacier marine front, most likely limits their ability to provide a realistic response to ocean forcing. The model that captured the observed retreat of the front position and associated inland draw down [e.g., *Hughes*, 1986; *Joughin et al.*, 2004] is the shallow ice model UMISM that approximately incorporated the effect of longitudinal shelf stresses via a Weertman style spreading rate at the ice front. Thus, the current generation of Greenland whole ice sheet models is not yet able to simulate the potential response to a warming ocean, and caution is needed when interpreting the SeaRISE response to this scenario, as the ensemble mean response likely underestimates the true potential response. Capturing the evolution of the ice front position and its associated effect on the dynamics of the ice sheet remains a challenge for whole ice sheet models that can only be addressed with an increased understanding of ice-ocean interactions and the treatment of marine boundaries (grounding line migration or calving front and rates). Progress can be made by subjecting ice sheet models to intercomparison exercises that specifically target the behavior of marine terminating ice fronts, such as the existing Marine Ice Sheet Model

Intercomparison Project (MISMIP) and Marine Ice Sheet Model Intercomparison Project for planview models (MISMIP3d) efforts that focus on grounding line migration [*Pattyn et al.*, 2012; *Pattyn et al.*, 2013]. The positive feedback between the thinner outlet glacier termini and surface mass balance and its potential to alter the flow of ice streams indicate the need for two-way coupling of dynamic ice sheet models to climate models in order to refine the quantitative projections of future sea levels.

[51] Spatial analysis of the thickness response to the SeaRISE external forcings based on the unweighted ensemble mean and standard deviation thus significantly adds to the bulk numbers of sea level contribution [*Bindschadler et al.*, 2013], by identifying aspects where ice sheet models agree on a regional scale. The approach also identifies where models disagree [*Knutti et al.*, 2010b], as reflected in the scatter in model responses in the central west basin due to Jakobshavn Isbrae, for example. The spread in the multimodel ensemble can help to characterize the uncertainty in the simulations through understanding the sources of the variations across the ensemble members [*Knutti et al.*, 2010a], and thus where model improvements in tandem with observations, as discussed in this conclusion, are still needed. Just as in any future climate simulation, the uncertainty in the SeaRISE simulations arises due to the uncertainty in the initial conditions and the uncertainty in determining future climate forcing scenarios. Obtaining an initial configuration that is in agreement with the present-day conditions, but that also captures the transients due to previous climatic conditions, is a particular problem. The uncertainties in the simulated responses are also due to observational uncertainty, such as the ice thickness or the basal conditions beneath the ice sheets (e.g., bed topography, geothermal heat flux). Uncertainty in model physics, for example, in the sliding relations, and structural uncertainty (processes that cannot be resolved due to computational constraints) also affect the responses shown in this work. Unfortunately, every ice sheet model suffers from these uncertainties, so it is very difficult to identify a single model that should be trusted in preference to the other models. Reducing the uncertainty in the ensemble simulations can potentially be achieved by assigning weights to the models, or by using a subset of models. However, this requires a robust and reliable method for evaluating the projection skills of ice sheet models, a task that has proven challenging with climate models [e.g., *Gleckler et al.*, 2008; *Knutti et al.*, 2010a]. To facilitate these future efforts, the outputs from the SeaRISE sensitivity experiments will be made publicly available. Future investigations such as SeaRISE could potentially assign weights by requiring ice sheet models to reproduce the recently observed ice sheet losses, but for this to be successful would also require precise determination of the forcings driving the changes. Progress toward reducing the uncertainties in ice sheet projections is crucial as ice sheets influence our future sea levels and are thus an issue of enormous societal importance.

Appendix A: Model Descriptions

[52] This appendix summarizes in Table A1 the essential features of the ice models taking part in the Greenland SeaRISE suite of experiments, along with the implementation of the forcings. The models often have additional capabilities that are not used in the SeaRISE experiments and therefore not included in Table A1.

Table A1. Characteristics of Greenland Models Used in SeaRISE

Model	IcIES	Elmer/Ice	UMISM	ISSM
Numerical method	Finite difference, Eulerian	Finite element with triangular prisms, Eulerian	Finite element quadrilaterals	Finite element; arbitrary Lagrangian Eulerian (ALE)
Grid (horizontal; vertical)	H: uniform 10 km V: 26 layers (terrain-following)	H: Adaptive (between 1 km on the margins and 70 km in the interior) V:17 layers (terrain-following)	H: 10 km V:40 layers, nonuniformly spaced	H: Anisotropic (between 3 km on fast ice streams and 15 km in the interior) V: 14 layers nonuniformly spaced
Time step	Adaptive, maximum of 0.125 years	1 month	1 year	2 months
Spin-up/initialization	One glacial cycle from 125 ka steady state	Initial spin-up (from the Eemian through the last glacial period until 200 B.P.) with the shallow-ice model SICOPOLIS using fixed, slightly smoothed present-day topography. Final relaxation (from 200 BP until the present) with Elmer/Ice	30,000 year, driven by ice core temperature proxy	Data assimilation to match present-day velocities and self-consistent temperature field
Ice flow mechanics	Shallow ice	Full Stokes	Shallow ice	Higher-order (Blatter-Pattyn)
Surface mass balance and temperature	PDD by *Reeh* [1991] with temperature-dependent PDD factors following *Tarasov and Peltier* [2002].	Present-day mean annual and mean summer surface temperatures by *Fausto et al.* [2009]; present-day accumulation by *Ettema et al.* [2009]; PDD by *Reeh* [1991] with factors of 8 mm/(d K) for ice melt and 3 mm/(d K) for snow melt	Mean annual temperature (MAT) from latitudinal and elevation lapse rates [*Fausto et al., 2009*] PDD with latitude-dependent amplitude around MAT	SeaRISE data sets as no PDD scheme
Basal sliding	Weertman sliding law (m = 3), experiment amplifies the sliding coefficient	Weertman sliding law with basal temperature dependence (p = 3, q = 2). Experiment reduces the basal drag	Nonlinear Weertman sliding law; lubrication factor proportional to basal water amount; experiment amplifies the lubrication factor	Linear viscous sliding law; experiment reduces the sliding coefficient
Basal hydrology	None	None	Basal water conserved; source calculated from basal melting	None
Ice shelves	No; melting experiment applies melt rates to ice front where the bed is below sea level	No; no participation in melting experiment	No, but effect of ice shelf approximated by imposing at the grounding line *Weertman's* [1974] thinning rate and *Thomas'* (1973) back stress; melting experiment applies melt rates at last grounded grid point	No, since SeaRISE Greenland mask data set does not contain ice shelves; melting applied on fixed ice front where the ice thickness is at hydrostatic equilibrium, the bed below sea-level and the ice front adjacent to water; once ice front thickness has melted away, the melting stops, and changes are due to ice dynamics
Grounding line (GL) advance/retreat	GL is determined by a floating criterion: when thickness at a grid is below flotation thickness, then immediately cut off	GL is fixed	Grounding limit shifts to position where surface falls below flotation height	Fixed calving front and GL
References	*Saito and Abe-Ouchi* [2004,2005,2010], *Greve et al.* [2011]	*Seddik et al.* [2012]	*Fastook* [1993]	*Morlighem et al.* [2010], *Seroussi et al.* [2011], *Larour et al.* [2012a, 2012b]

Table A1. (continued)

Characteristics/Model	SICOPOLIS Greenland	PISM	AIF	CISM 2.0
Numerical method	Finite difference, Eulerian	Finite difference, Eulerian	Finite difference, Eulerian	Finite difference, Eulerian, explicit mass, and tracer advection (using incremental remapping)
Grid (horizontal; vertical)	H: 5 km; V: 91 layers (terrain-following)	H: 5 km; V: 10 m, equally spaced	H: 40 km average grid spacing; V: 20 evenly spaced layers	H: uniform 5km; V: 11-level sigma coordinate
Time step	Thickness, velocity: 0.1–0.2 year; temperature: 0.1–0.2 year.	Adaptive, typically about 15 days	1 year	0.1–0.2 years as required for numerical stability
Spin-up/initialization	First 125 ka steady state, then 125 ka transient (from the Eemian through the last glacial period until present); with fixed, slightly smoothed present-day topography	125 ka transient (from the last glacial period until present)	Iteration on the governing equations with the present-day ice sheet geometry and climate forcing; the balance velocity is used as the target to tune the stress configuration through an adjustable enhancement factor	Quasi-steady state spin-up to bring energy and momentum balance into approximate equilibrium with present-day geometry; basal sliding parameters tuned to match balance velocities
Ice flow mechanics	Shallow ice	Shallow ice + shelf stream (hybrid)	Higher-order with longitudinal and vertical shear stresses	First-order (Blatter/Pattyn)
Surface mass balance and temperature	Present-day mean annual and mean summer surface temperatures by *Fausto et al.* [2009]; present-day accumulation by *Ettema et al.* [2009]; PDD by *Reeh* [1991] with factors of 8 mm/(d K) for ice melt and 3 mm/(d K) for snow melt	PDD with European Ice Sheet Modeling Initiative Greenland parameters [*Huybrechts*, 1998]	SeaRISE-provided mean annual temperature; positive degree day method using SeaRISE suggested parameters	SeaRISE-provided mean annual temperature and surface forcings
Basal sliding	Weertman sliding law with basal temperature dependence (p=3, q=2); experiment amplifies the sliding coefficient	Nearly plastic power law [*Schoof and Hindmarsh*, 2010]; experiment reduces the basal friction coefficient	Weertman sliding law (m=3); experiment amplifies the sliding coefficient	Linear viscous (using MacAyeal-type "beta-squared" sliding law); experiment reduces the basal friction coefficient
Basal hydrology	Water content computed in near-basal temperate ice (max. 1%), basal melting rate computed under grounded ice	Basal meltwater model: controls bed strength	None	None
Ice shelves	No for Greenland; melting applied at grounded ice cells that have a base below sea-level and are adjacent to ocean	No; no participation in melting experiment	No; melting applied to the perimeter grid points with a bed below sea level	No; no participation in melting experiment
Advance/retreat	Freely evolving ice margin based on the flotation condition, but limited to the present-day extent	Fixed calving front	Ice sheet margin moves freely; grounding line detected by the floatation condition	Calving front and terrestrial margin allowed to retreat (if thin to zero) but not advance past present-day margin position
References	*Greve et al.* [2011], *Sato and Greve* [2012]	*Bueler and Brown* [2009], *Aschwanden et al.* [2012]	*Wang et al.* [2012]	*Price et al.* [2011]; *Lemieux et al.* [2011]; *Evans et al.* [2012]; *Bougamont et al.* [2012]

References

Aschwanden, A., E. Bueler, C. Khroulev, and H. Blatter (2012), An enthalpy formulation for glaciers and ice sheets, *J. Glaciol.*, *58*(209), 441–457.

Bamber, J. L., R. L. Layberry, and S. P. Gogineni (2001a), A new ice thickness and bed data set for the Greenland ice sheet 1: Measurement, data reduction, and errors, *J. Geophys. Res.*, *106*(D24), 33773–33780.

Bamber, J. L., R. L. Layberry, and S. P. Gogineni (2001b), A new ice thickness and bed data set for the Greenland ice sheet 2: Relationship between dynamics and basal topography, *J. Geophys. Res.*, *106*(D24), 33781–33788.

Bartholomew, I., P. Nienow, D. Mair, A. Hubbard, M. A. King, and A. Sole (2010), Seasonal evolution of subglacial drainage and acceleration in a Greenland outlet glacier, *Nat. Geosci.*, *3*, 408–411.

Bindschadler, R., et al. (2013), Ice-sheet model sensitivities to environmental forcing and their use in projecting future sea-level (the SeaRISE Project), *J. Glaciol.*, *50*, 195–224, doi:10.3189/2013JoG12J125.

Bougamont, M., S. Price, P. Christoffersen, and A. J. Payne (2012), Dynamic patterns of ice stream flow in a 3-D higher-order ice sheet model with plastic bed and simplified hydrology, *J. Geophys. Res.*, *116*, F04018, doi:10.1029/2011JF002025.

Box, J. E., and K. Steffen (2001), Sublimation on the Greenland ice sheet from automated weather station observations, *J. Geophys. Res.*, *106*(D24), 33965–33981.

Bueler, E., and J. Brown (2009), The shallow shelf approximation as a "sliding law" in a thermomechanically coupled ice sheet model, *J. Geophys. Res.*, *114*, F03008, doi:10.1029/2008JF001179.

Burgess, E. W., R. R. Forster, J. E. Box, E. MoSLEy-Thompson, D. H. Bromwich, R. C. Bales, and L. C. Smith, (2010), A spatially calibrated model of annual accumulation rate on the Greenland ice sheet (1958–2007), *J. Geophys. Res.*, *115*, F02004, doi:10.1029/2009JF001293.

Das, S. B., I. Joughin, M. D. Behn, I. M. Howat, M. A. King, D. Lizarralde, and M. P. Bhatia (2008), Fracture propagation to the base of the Greenland ice sheet during supraglacial lake drainage, *Science*, *320*, 778–781.

Ettema, J., M. R. Van den Broeke, E. Van Meijgaard, W. J. Van de Berg, J. L. Bamber, J. E. Box, and R. C. Bales (2009), Higher surface mass balance of the Greenland ice-sheet revealed by high resolution climate modeling, *Geophys. Res. Lett.*, *36*, L12501, doi:10.1029/2009GL038110.

Evans, K. J., et al. (2012), A modern solver interface to manage solution algorithms in the Community Earth System Model, *Int. J. High Perf. Comp.*, *26*, 54–62.

Fastook, J. L. (1993), The finite-element method for solving conservation equations in glaciology, *Comp. Sci. Eng.*, *1*, 55–67.

Fastook, J. L., and T. J. Hughes (1990), Changing ice loads on the Earth's surface during the last glacial cycle, in *Glacial Isostasy, Sea-Level and Mantle Rheology, Series C: Mathematical and Physical Sciences*, Vol. *334*, 165–207, edited by R. Sabadini, K. Lambeck, and E. Boschi, Kluwer Academic Publishers, Dordrecht/Boston/London.

Fastook, J. L., and M. Prentice (1994), A finite-element model of Antarctica: Sensitivity test for meteorological mass balance relationship, *J. Glaciol.*, *40*, 167–175.

Fausto, R. S., A. P. Ahlstrom, D. Van As, C. E. Boggild, and S. J. Johnsen (2009), A new present-day temperature parameterisation for Greenland, *J. Glaciol.*, *55*, 95–105.

Gates, W. L., et al. (1999), An overview of the results of the Atmospheric Model Intercomparison Project (AMIP I), *Bull. Am. Meteor. Soc.*, *80*, 29–55.

Giorgi, F. (2005), Interdecadal variability of regional climate change: Implications for the development of regional climate change scenarios, *J. Meteorol. Atmos. Phys.*, *89*, 1–15.

Gleckler, P. J., K. E. Taylor, and C. Doutriaux (2008), Performance metrics for climate models, *J. Geophys. Res.*, *113*, D06104, doi:10.1029/2007JD008972.

Greve, R. (1997), A continuum-mechanical formulation for shallow polythermal ice sheets, *Phil. Trans. Roy. Soc. Ser. A*, *355*, 921–974.

Greve, R., F. Saito, and A. Abe-Ouchi (2011), Initial results of the SeaRISE numerical experiments with the models SICOPOLIS and IcIES for the Greenland ice sheet, *Ann. Glaciol.*, *52*(58), 23–30, doi:10.3189/172756411797252068.

Herzfeld, U. C., J. L. Fastook, B. Greve, R. McDonald, B. F. Wallin, and P. A. Chen (2012), On the influence of Greenland outlet glacier bed topography on results from dynamic ice sheet models, *Ann. Glaciol.*, *53*(60), 281–293.

Holland, D. M., R. H. Thomas, B. de Young, M. H. Ribergaard, and B. Lyberth (2008), Acceleration of Jakobshavn Isbrae triggered by warm subsurface ocean waters, *Nat. Geosci.*, *1*, 659–664.

Howat, I. M., and A. Eddy (2011), Multi-decadal retreat of Greenland's marine-terminating glaciers, *J. Glaciol.*, *57*(203), 389–396.

Howat, I., I. Joughin, and T. A. Scambos (2007), Rapid changes in ice discharge from Greenland outlet glaciers, *Science*, *315*, 1559–1561.

Howat, I. M., S. Tulaczyk, E. Waddington, and H. Bjornsson (2008), Dynamic controls on glacier basal motion inferred from surface ice motion, *J. Geophys. Res. 113*, F03015, doi:10.1029/2007JF000925.

Hughes, T. (1986), The Jakobshavn effect, *Geophys. Res. Lett.*, *13*(1), 46–48.

Huybrechts, P. (1998), Report of the Third EISMINT Workshop on Model Intercomparison, European Science Foundation (Strasbourg), 120 p.

IPCC: Climate Change (2007), *The Physical Sciences Basis, Contribution of Working Group 1 to the Fourth Assessment Report of the Intergovernmental Panel on Climate Change*, edited by S. Solomon, D. Qin, M. Manning, Z. Chen, M. Marquis, K. B. Averyt, M. Tignor, and H. L. Miller, pp. 996, Cambridge University Press, Cambridge, UK and New York, NY, USA.

Johnsen, S. J., D. Dahl-Jensen, W. Dansgaard, and N. Gundestrup (1995), Greenland palaeotemperatures derived from GRIP borehole temperature and ice core isotope profiles, *Tellus*, *47B*(5), 624–629.

Joughin I., W. Abdalati, and M. Fahnestock (2004), Large fluctuations in speed on Greenland's Jakobshavn Isbræ glacier, *Nature*, *432*, 608–610, doi:10.1038/nature03130.

Joughin, I., S. B. Das, M. A. King, B. E. Smith, I. M. Howat, and T. Moon (2008a), Seasonal speedup along the western flank of the Greenland ice sheet, *Science*, *320*(5877), 781–783.

Joughin, I., I. Howat, R. B. Alley, G. Ekstrom, M. Fahnestock, T. Moon, M. Nettles, M. Truffer, and V. C. Tsai (2008b), Ice-front variation and tidewater behavior on Helheim and Kangerdlugssuaq Glaciers Greenland, *J. Geophys. Res.*, *113*(F1), F01004, doi:10.1029/2007JF000837

Joughin I., B. E. Smith, I. M. Howat, T. Scambos, and T. Moon (2010), Greenland flow variability from ice-sheet wide velocity mapping, *J. Glaciol.*, *56*(197), 415–430.

Joughin I., B. E. Smith, I. M. Howat, D. Floricioiu, D. Alley, M. Truffer, and M. Fahnestock (2012), Seasonal to decadal scale variations in the surface velocity of Jakobshavn Isbrae, Greenland: Observation and model-based analysis, *J. Geophys. Res.*, *117*, F02030, doi:10.1029/2011JF002110.

Knutti, R., G. Abramowitz, M. Collins, V. Eyring, P. J. Gleckler, B. Hewitson, and L. Mearns (2010a), Good practice guidance paper on assessing amd combining multi model climate projections, in *Meeting Report of the Intergovernmental Panel on Climate Change Expert Meeting on Assessing and Combining Multi Model Climate Projections*, pp. 13, edited by T. F. Stocker, D. Qin, G. K. Plattner, M. Tignor, and P. M. Midgley, IPCC Working Group I Technical Support Unit, University of Bern, Bern, Switzerland.

Knutti, R., R. Furrer, C. Tebaldi, J. Cermak, and G. A. Meehl (2010b), Challenges in combining projections from multiple climate models, *J. Climate*, *23*, 2739–2758, doi:10.1175/2009JCLI3361.1.

Larour, E., J. Schiermeier, E. Rignot, H. Seroussi, and M. Morlighem (2012a), Sensitivity analysis of Pine Island Glacier ice flow using ISSM and DAKOTA, *J. Geophys. Res.*, *117*, F02009, doi:10.1029/2011JF002146.

Larour, E., H. Seroussi, M. Morlighem, and E. Rignot (2012b), Continental scale, high order, high spatial resolution, ice sheet modeling using the Ice Sheet System Model (ISSM), *J. Geophys. Res.*, *117*, F01022, doi:10.1029/2011JF002140.

Lemieux, J. F., S. F. Price, K. J. Evans, D. Knoll, A. G. Salinger, D. M. Holland, and A. J. Payne (2011), Implementation of the Jacobian-free Newton-Krylov method for solving the first-order ice sheet momentum balance, *J. Comp. Phys.*, *230*, 6531–6545.

Lipscomb, W., R. Bindschadler, E. Bueler, D. Holland, J. Johnson, and S. Price (2009), A community ice sheet model for sea level prediction, *Eos Trans.*, *90*(3), 23.

Little, C. M., et al. (2007), Toward a new generation of ice sheet models, *Eos Trans.*, *88*, 578.

Luckman, A., T. Murray, R. de Lange, and E. Hanna (2006), Rapid and synchronous ice-dynamic changes in East Greenland, *Geophys. Res. Lett.*, *33*, L03503, doi:10.1029/2005GL025428.

MacAyeal, D. (1989), Large-scale ice flow over a viscous basal sediment: Theory and application to ice stream B, Antarctica, *J. Geophys. Res.*, *94*(B4), 4071–4087.

Moon, T., I. Joughin, B. Smith, and I. Howat (2012), 21st-century evolution of Greenland outlet glacier velocities, *Science*, *336*, 576–578.

Morlighem, M., E. Rignot, H. Seroussi, E. Larour, H. Ben Dhia, and D. Aubry (2010), Spatial patterns of basal drag inferred using control methods from a full-Stokes and simpler models for Pine Island Glacier, West Antarctica, *Geophys. Res. Lett.*, *37*, L14502, doi:10.1029/2010GL043853.

Parizek, B. R., and R. B. Alley (2004), Implications of increased Greenland surface melt under global-warming scenarios: Ice-sheet simulations, *Quat. Sci. Rev.*, *23*, 1013–1027.

Pattyn, F., et al. 2012, Results of the Marine Ice Sheet Model Intercomparison Project MISMIP, *The Cryosphere Discuss.*, *6*, 267–308, doi:10.5194/tcd-6-267-2012.

Pattyn, F., et al. (2013), Grounding-line migration in plan-view marine ice-sheet models: Results of the ice2sea MISMIP3d intercomparison, *J. Glaciol.*, *59*(215), 410–422, doi:10.3189/2013JoG12J129

Payne, A. J., P. R. Holland, A. P. Shepherd, I. C. Rutt, A. Jenkins, and I. Joughin (2007), Numerical modeling of ocean-ice interactions under Pine Island Bay's ice shelf, *J. Geophys. Res.*, *112*, C10019, doi:10.1029/2006JC003733.

Price, S. F., A. J. Payne, I. M. Howat, and B. E. Smith (2011), Committed sea-level rise for the next century from Greenland ice sheet dynamics during the past decade, *Proc. Nat. Acad. Sci.*, *108*, 8978–8983.

Pritchard, H., R. Arthern, D. Vaughan, and L. Edwards (2009), Extensive dynamic thinning on the margins of the Greenland and Antarctic ice sheets, *Nat. Lett.*, *461*, 971–975.

Reeh, N., (1991), Parameterization of melt rate and surface temperature on the Greenland ice sheet. *Polarforschung*, *59*(3), 113–128.

Rignot, E., and P. Kanagaratnam (2006), Changes in the velocity structure of the Greenland ice sheet, *Science*, *311*, 986–990.

Rignot, E., I. Velicogna, M. R. van den Broeke, A. Monaghan, and J. Lenaerts (2011), Acceleration of the contribution of the Greenland and Antarctic ice sheets to sea level rise, *Geophys. Res. Lett.*, *38*, L05503, doi:10.1029/2011GL046583

Rogozhina, I., Z. Martinec, J. M. Hagedoorn, M. Thomas, and K. Fleming (2011), On the long term memory of the Greenland ice sheet, *J. Geophys. Res.*, *116*, F01011, doi:10.1029/2010JF001787.

Sato, T., and R. Greve (2012), Sensitivity experiments for the Antarctic ice sheet with varied sub-ice-shelf melting rates, *Ann. Glaciol.*, *53*(60), 221–228, doi:10.3189/2012AoG60A042

Saito, F., and A. Abe-Ouchi (2004), Thermal structure of Dome Fuji and east Dronning Maud Land, Antarctica, simulated by a three-dimensional ice-sheet model, *Ann. Glaciol.*, *39*, 433–438.

Saito, F., and A. Abe-Ouchi (2005), Sensitivity of Greenland ice sheet simulation to the numerical procedure employed for ice sheet dynamics, *Ann. Glaciol.*, *42*, 331–336.

Saito, F., and A. Abe-Ouchi (2010), Modelled response of the volume and thickness of the Antarctic ice sheet to the advance of the grounded area, *Ann. Glaciol.*, *51*, 41–48.

Schoof, C. (2010), Ice sheet acceleration driven by melt supply variability, *Nature*, *468*(7325), 803–806, doi:10.1038/nature09618.

Schoof, C., and R. C. A. Hindmarsh (2010), Thin-film flows with wall slip: An asymptotic analysis of higher order glacier flow models. *Q. J. Mech. Appl. Math.*, *63*(1), 73–114, doi:10.1093/qjmam/hbp025

Seddik, H., R. Greve, T. Zwinger, F. Gillet-Chaulet, and O. Gagliardini (2012), Simulations of the Greenland ice sheet 100 years into the future with the full Stokes model Elmer/Ice, *J. Glaciol.*, *58*(209), 427–440.

Seroussi, H., M. Morlighem, E. Rignot, E. Larour, D. Aubry, H. Ben Dhia, and S. S. Kristensen (2011), Ice flux divergence anomalies on 79 north glacier, Greenland, *Geophys. Res. Lett.*, *38*, L09501, doi:10.1029/2011GL047338.

Shapiro, N. M., and M. H. Ritzwoller (2004), Inferring surface heat flux distributions guided by a global seismic model: Particular application to Antarctica, *Earth Planet. Sci. Lett.*, *223*, 213–224.

Shepherd, A., A. Hubbard, P. Nienow, M. King, M. McMillan, and I. Joughin (2009), Greenland ice sheet motion coupled with daily melting in late summer, *Geophys. Res. Lett.*, *36*, L01501, doi:10.1029/2008GL035758.

Shepherd, A., et al. (2012), A reconciled estimate of ice-sheet mass balance. *Science*, *338*(6111), 1183–1189, doi:10.1126/science.1228102

Stearns L. A., and G. S. Hamilton (2007), Rapid volume loss from two East Greenland outlet glaciers quantified using repeat stereo satellite imagery, *Geophys. Res. Lett.*, *34*, L05503 doi:10.1029/2006GL028982

Stephenson, D. B., C. A. S. Coelho, F. J. Doblas-Reyes, and M. Balmaseda (2005), Forecast assimilation: A unified framework for the combination of multi-model weather and climate predictions, *Tellus A*, *57*, 253–264.

Stone E., D. Lunt, I. Rutt, and E. Hanna (2010), Investigating the sensitivity of numerical model simulations of the modern state of the Greenland ice-sheet and its future response to climate change, *Cryosphere*, *4*, 397–417.

Tarasov, L., and W. R. Peltier (2002), Greenland glacial history and local geodynamic consequences, *Geophys. J. Int.*, *150*(1), 198–229, doi:10.1046/j.1365-246X.2002.01702.x.

Thomas, R. H. (1973), The creep of ice shelves: Theory, *J. Glaciol.*, *12*(64), 45–53.

van der Veen, C. J., and A. J. Payne (2004), Modelling land-ice dynamics, in *Mass Balance of the Cryosphere Observations and Modelling of Contemporary and Future Changes*, edited by J. L. Bamber, and A. J. Payne, pp. 169–219, Cambridge University Press, Cambridge UK.

van der Veen, C. J., D. H. Bromwich, B. Csatho, and C. Kim (2001), Trend analysis of Greenland precipitation, *J. Geophys. Res.*, *106*(D24), 33909–33918.

Velicogna, I. (2009), Increasing rates of ice mass loss from the Greenland and Antarctic ice sheets revealed by GRACE, *Geophys. Res. Lett.*, *36*, L19503, doi:10.1029/2009GL040222.

van de Wal, R. S. W., W. Boot, M. R. van den Broeke, C. J. P. P. Smeets, C. H. Reijmer, J. J. A. Donker, and J. Oerlemans (2008), Large and rapid melt-induced velocity changes in the ablation zone of the Greenland ice sheet, *Science 321*, 111–113.

van den Broeke, M., J. Bamber, J. Ettema, E. Rignot, E. Schrama, W. J. van de Berg, W.E. van Meijgaard, I. Velicogna, and B. Wouters (2009), Partitioning recent Greenland mass loss, *Science*, *326*(5955), 984–986, doi:10.1126/science.1178176

Vieli, A., and F. M. Nick (2011), Understanding and modeling rapid dynamical changes of tidewater outlet glaciers: issues and implications. *Surv. Geophys.*, *32*(4–5), 437–458, doi:10.1007/s10712-011-9132-4

Wang, W., J. Li, and J. Zwally (2012), Dynamic inland propagation of thinning due to ice loss at the margins of the Greenland ice sheet, *J. Glaciol.*, *58*(210), 734–740.

Weertman, J. (1974), Stability of the junction of an ice sheet and an ice shelf, *J. Glaciol.*, *13*(67), 3–11.

Weigel, A. P., R. Knutti, M. A. Liniger, and C. Appenzeller (2010), Risks of model weighting in multimodel climate projections, *J. Climate*, *23*(15), 4175–4191.

Williams, M. J. M., K. Grosfeld, R. C. Warner, R. Gerdes, and J. Determann (2001), Ocean circulation and ice-ocean interaction beneath the Amery Ice Shelf, Antarctica, *J. Geophys. Res.*, *106*(C10), 22383–22399.

Zwally H. J., W. Abdalati, T. Herring, K. Larson, J. Saba, and K. Steffen (2002), Surface melt-induced acceleration of Greenland ice-sheet flow, *Science*, *297*(5579), 218–222.

Zwally, H. J., et al. (2011), Greenland ice sheet mass balance: Distribution of increased mass loss with climate warming; 2003–07 versus 1992–2002, *J. Glaciol.*, *57*(201), 88–102.